Astronomy & Astrophysics

H I line observations of 2MASS galaxies in the zone of avoidance[⋆,⋆⋆]

W. van Driel[1,2], S. E. Schneider[3], R. C. Kraan-Korteweg[4], and D. Monnier Ragaigne[5]

[1] GEPI, Observatoire de Paris, CNRS, Université Paris Diderot, 5 place Jules Janssen, 92190 Meudon, France
e-mail: wim.vandriel@obspm.fr
[2] Station de Radioastronomie de Nançay, Observatoire de Paris, CNRS/INSU, 18330 Nançay, France
[3] University of Massachusetts, Astronomy Program, 536 LGRC, Amherst, MA 01003, USA
e-mail: schneide@messier.astro.umass.edu
[4] Department of Astronomy, University of Cape Town, Private Bag X3, Rondebosch 7701, South Africa
e-mail: kraan@ast.uct.ac.za
[5] Laboratoire de l'Accélérateur Linéaire, Université Paris-Sud, Bâtiment 200, BP 34, 91898 Orsay Cedex, France
e-mail: monnier@lal.in2p3.fr

ABSTRACT

Aims. A pilot survey has been made to obtain 21 cm H I emission line profiles for 197 objects in the zone of avoidance (ZoA) that were classified as galaxies in the 2MASS all-sky near-infrared Extended Source Catalog (2MASX), as well as a further 16 2MASS pre-release working database sources that did not make it into 2MASX.
Methods. One hundred sixteen of the 2MASX sources and the 16 working database sources were observed using the Nançay radio telescope, usually in the 325 to 11 825 km s^{-1} range, and the other 81 2MASX sources were observed with the Arecibo radio telescope in the –500 to 11 000 km s^{-1} range, and for 9 also in the 9500 to 21 000 km s^{-1} range.
Results. Global H I line parameters are presented for the 22 and 29 2MASX objects that were detected at Nançay and Arecibo, respectively, as well as upper limits for the undetected 2MASX objects. Another galaxy (ESO 371-27) was detected in the Nançay beam centred on an undetected target, ESO 371-26. Nançay data on 12 sources could not be used due to high rms noise levels, most likely caused by strong nearby continuum sources. None of the 16 working database sources were detected at Nançay. Whereas object 2MASX J08170147-3410277 appears to be a very massive galaxy with an H I mass of 4.6×10^{10} $M_\odot$ and an inclination-corrected rotation velocity of 314 km s^{-1}, it is clear that only radio synthesis H I imaging observations will allow a firm conclusion on this.
Conclusions. Overall, the global properties of the detected galaxies match those of other ZoA H I surveys. Although the detections are as yet too sparse to give further insight into suspected or unknown large-scale structures in the ZoA, they already indicate that an extension of the present pilot survey is bound to quantify filaments, clusters, and voids behind this part of the Milky Way. It is shown that the number of candidate 2MASS-selected ZoA galaxies to be observed in H I could have been reduced by about 15% through examination of composite near-infrared images and the application of extinction-corrected near-infrared colour limits. Present results confirm that the Galactic extinction values from Schlegel et al. (1998) are valid for latitudes $|b| \gtrsim 5°$, but increasingly less so for lower latitudes.

Key words. galaxies: distances and redshifts – galaxies: general – galaxies: ISM – infrared: galaxies – radio lines: galaxies

1. Introduction

Because of dust extinction at low Galactic latitudes, resulting in the so-called zone of avoidance (ZoA), redshift surveys have generally concentrated on regions farther than 10° from the Galactic plane (e.g. Kraan-Korteweg & Lahav 2000), except for systematic H I surveys (e.g. HIPASS, Meyer et al. 2004) and systematic H I ZoA at $|b| \leq 5°$ (Henning et al. 2000a,b; Donley et al. 2005; Kraan-Korteweg 2005). This has left a gap

in our knowledge of local large-scale structure over a large part of the sky – see, e.g., Fig. 10. The existence and membership of nearby groups of galaxies is still highly uncertain and even dwarfs within the Local Group keep being detected at low latitudes. We have collected 21 cm H I line data of near-infrared selected galaxies with unknown redshifts in the ZoA ($|b| \leq 10°$), mostly focusing on objects with relatively large angular size that are likely to be nearby, to reduce the redshift ZoA and complement the various existing all-sky (redshift) surveys.

The interstellar extinction in the K_s-band (2.2 μm) is 12 times smaller than in the *B*-band and 5.5 times smaller than in the *I*-band (Cardelli et al. 1989). We therefore decided to select probable ZoA galaxies from the – at that time (in 2000–2002) – emerging systematic 2-Micron All Sky Survey (2MASS, Skrutskie et al. 2006). Many of these ZoA galaxies are invisible on the Palomar Sky Survey (DSS) images and even in the *I*-band have several magnitudes of extinction, whereas the extinction in

---
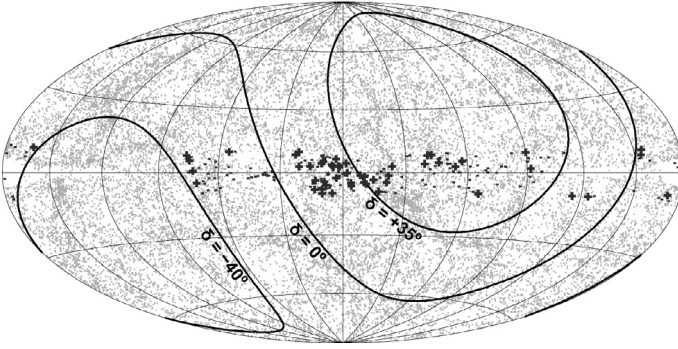
Fig. 1. All-sky plot of bright ($K_s \leq 11\overset{m}{.}4$) 2MASS extended sources. The galaxy positions (grey dots) are plotted in Galactic coordinates, centred on the Galactic anticentre. The black dots indicate galaxies observed in this project, and the + symbols indicate galaxies whose H I signal was detected.

the K_s-band remains relatively modest in most cases. Follow-up H I-observations of these heavily absorbed galaxies are then the most efficient – if not only – tool to obtain a distance estimate and map large-scale structures across the ZoA.

Nevertheless, identification of galaxies at very low Galactic latitudes remains difficult even using 2MASS, not so much because of dust extinction, but due to stellar crowding close to the Galactic plane. In particular, the wider Galactic Bulge area makes the automatic identification of extended sources increasingly uncertain, or even impossible when star densities of $\log N = 4.00/(\deg)^2$ are reached for stars with $K \leq 14\overset{m}{.}0$, leading to the so-called NIR ZoA (see Fig. 9 in Kraan-Korteweg 2005).

2MASS used two identical telescopes in the north and the south to observe the entire sky at J, H, and K_s, providing an opportunity to select a much more uniform sample of galaxies than has been possible previously. Note that although we initially used the 2000 and 2002 versions of the working database for our source selection, all data presented here are updated to the final release catalogue values. Figure 1 shows an all-sky map of 2MASS-selected bright ($K_s \leq 11\overset{m}{.}4$), extended sources in Galactic coordinates (centred on the Galactic anti-centre direction), demonstrating that we can select sources quite uniformly deep into the ZoA. The heavy curves in the figure show declinations of –40°, 0°, and +35° which correspond to the declination limits of the radio telescopes (Nançay and Arecibo; see Sect. 2 for further details) used in this pilot project of observing 2MASS-selected ZoA galaxies in H I.

2MASS has a 95% completeness level of $K_s < 13\overset{m}{.}5$ at high Galactic latitudes (Jarrett et al. 2000), and has little dust extinction at low latitudes. However, close to the Galactic plane, the numerous faint (red) foreground stars effectively create a high sky-brightness noise level, and the fainter (low surface brightness) galaxies are extremely difficult to detect because of confusion noise. We therefore preferentially selected galaxies with $K_s < 12\overset{m}{.}0$ where the 2MASS galaxy sample still remains essentially complete (cf. Huchra et al. 2005). A $K_s = 12\overset{m}{.}0$ completeness limits corresponds to an optical B-band magnitude limit of $16\overset{m}{.}0$ to $14\overset{m}{.}0$ respectively, for typical $B-K$ galaxy colours ranging from about $4\overset{m}{.}0$ for ellipticals to $2\overset{m}{.}0$ for spirals (e.g., Jarrett et al. 2003).

In practice, a $K_s = 12\overset{m}{.}0$ selection was possible for the Nançay sample only, where 92% meet this criterion, whereas finding enough sources not yet observed in H I in the considerably smaller area observable at Arecibo resulted in selecting fainter sources, 93% of which have $K_s > 12\overset{m}{.}0$.

It should be emphasized here, however, that a NIR selected ZoA galaxy sample may not necessarily be identical to objects selected at high Galactic latitudes. It likely is biased in the sense that such a survey favours galaxies with higher (redder) surface brightness, or shorter scale lengths, hence early type or bulge-dominated spirals, against low surface brightness bluer galaxies. This is difficult to determine directly because of uncertainties in estimates of Galactic extinction and stellar subtraction. In fact, this is already playing a role at high Galactic latitudes where 2MASX underestimates magnitudes of galaxies by $0\overset{m}{.}2$ to $2\overset{m}{.}5$ (for total magnitudes) due to the loss of other LSB features of extended dwarf galaxies, hence being increasingly incomplete for LSB galaxies, and fails to detect the lowest LSB galaxies entirely (Kirby et al. 2008; Andreon 2002).

The near-infrared is less affected by a galaxy's star-formation history. A K_s-selected sample therefore provides a more accurate indication of the total stellar content of the galaxies, and is, for instance, less biased by galaxy interactions which can trigger star formation. Collecting redshifts and H I parameters for these galaxies, in particular in the ZoA, also contributes to broader efforts to build complete all sky samples of bright 2MASS galaxies, such as the 2MASS Redshift Survey (2MRS, see Huchra et al. 2005). Future studies can use the results from the present project to systematically identify a subset of 2MASS ZoA galaxies with good H I characteristics, such as appropriate inclinations and strong H I emission, that will allow the determination of peculiar velocities based on the NIR Tully-Fisher (TF) relation, and will complement ongoing efforts by Masters et al. (2008) for the whole sky 2MASS Tully Fisher relation survey (2MTF). In combination with the large-scale structure information provided by the 2MRS, such a survey will allow a significant improvement over dipole anisotropy derivations as well as reconstructed density and velocity fields from the 2MASS Redshift Survey (Erdogdu et al. 2006a,b) for which the lack of data in the ZoA still remains one of the major contributors to the uncertainties in understanding the dynamics in the nearby Universe as well as the Local Group (Loeb & Narayan 2008).

This paper is structured as follows: the selection of the sample of 2MASS ZoA galaxies observed by us in H I with the Nançay and Arecibo radio telescopes is described in Sect. 2, the observations and the data reduction are presented in Sect. 3, and the results in Sect. 4. A discussion of the results is given in Sect. 5 and the conclusions are presented in Sect. 6.

2. Sample selection

2.1. Nançay sample

At Nançay, we surveyed the ZoA within ±10° of the Galactic plane in the declination zones of –39° to 0°, and +35° to +73° (+73° being the northernmost limit of the ±10° latitude band around the Galactic plane). The reason for the exclusion of the declination range 0° to +35° is obviously due to the Arecibo telescope being much more efficient in capturing galaxies there. This leads to a Galactic longitude coverage of selected objects in the ZoA of about ℓ: –20° (340°) to 170° and ℓ: 210° to 270°. It should also be pointed out that the majority of the galaxies observed in the northern zone of avoidance do not overlap too much with the systematic (blind) ZoA surveys pursued with the Parkes Multi-Beam Receiver in the south and its extension to the north ($|b| \leq 5°$) as well as the extension to higher latitudes around the Galactic Bulge (see Kraan-Korteweg et al. 2008, for survey details). Indeed we have very few detections in common (see Sect. 5.5, Fig. 10). This must be influenced by the fact that

2MASS has identified very few low latitude galaxies ($\lesssim \pm 5°$) in the southern sky, i.e. around the Galactic Bulge.

Using a 2002 pre-release version of the 2MASS working database, for Nançay we selected the 2MASS sources that were classified as galaxies with the largest angular radii ($>41\rlap{.}''8$ at 20 mag arcsec^{-2} in the K_s-band) within the region to be covered at Nançay ($\sim$3600 deg^2). This led to over 8000 galaxies with extinction-corrected $K_s < 12\rlap{.}^m0$. We selected the strongest candidate galaxies from among these based on the classification scheme used to identify galaxies among the extended sources in the 2MASS catalogue (Jarrett et al. 2000). This automated classification scheme used training sets of known objects to assign a probability of a source being a galaxy or other extended source based on shape, symmetry, colour and other catalogued parameters. We then chose the largest from among these sources, leaving 1448. We searched the NASA/IPAC extragalactic database (NED) for any matching sources within 3′ of the positions of these sources and found that 581 had been previously classified as galaxies, and 278 had published redshifts. Eliminating all sources with known redshifts, we selected the 300 largest remaining sources, 104 of which were previously classified as galaxies. The final selection of the 132 sources that were actually observed was made based on the availability of telescope time, in which we aimed to observed the largest galaxies first. Note that for a sample chosen at high latitudes with matching 2MASS criteria, 96% of the sources were previously catalogued in NED and all of these had measured redshifts.

The following 16 2MASS working database sources which we observed at Nançay did not make it into the final 2MASS source catalogue – none of them were detected: 002552+670925, 004129+600437, 022135+642636, 165630-324741, 171245-341722, 173137-361819, 173535-141928, 174604-253240, 180835-231312, 181804-044820, 181856-182017, 190102-140747, 201300+354137, 2105131+493946, 2105142+493950, and 234810+610154.

2.2. Arecibo sample

At Arecibo, we surveyed the ZoA galaxies ($|b| \leq 10°$) in the declination zone of $+12°$ to $+38°$. At the time of the Arecibo source selection (2000), the 2MASS working database did not yet cover the $0°$ to $+12°$ declination range observable at Arecibo. Due to constraints in the telescope time scheduling, the right ascension of the observed objects ranges from 20^h00^m to 06^h30^m, hence they mostly lie in the ZoA in the longitude range of about $\ell 170°$ to $210°$ plus a handful around $60°$.

In this zone, we observed 81 2MASS mostly low surface brightness sources, selected on a mean central K_s surface brightness in the inner 5″ radius of $K_5 \geq 18$ mag arcsec^{-2}, in the same manner as the 2MASS LSB objects selected outside the ZoA by Monnier Ragaigne et al. (2003a).

All but one of 2MASS working database sources observed at Arecibo made it into final version of the 2MASS extended source catalog; the one source that did not (0639299+170558) was not detected.

It is worthwhile pointing out that most of the selected galaxies are on average much fainter and smaller than the Nançay ZoA sample (see Fig. 5 in Sect. 5) despite these galaxies being mostly in an area of low extinction and star density (roughly the Galactic anti-centre). The reason for this is that the majority of the brighter galaxies had been identified before by Pantoja et al. (1994) by visual examination of POSS E prints in their efforts to search for optical galaxy candidates to trace the possible continuity across the Galactic plane of the southwestern spur

of the Perseus-Pisces complex. They had then used Arecibo for follow-up H I observations of the larger galaxies (Pantoja et al. 1997).

3. Observations and data reduction

All radial velocities in this paper, both H I and optical, are heliocentric and calculated according to the conventional optical definition ($V = c(\lambda-\lambda_0)/\lambda_0$).

3.1. Nançay observations and data reduction

The Nançay decimetric radio telescope, a meridian transit-type instrument of the Kraus/Ohio State design, consists of a fixed spherical mirror (300 m long and 35 m high), a tiltable flat mirror (200×40 m), and a focal carriage moving along a curved rail track. Sources on the celestial equator can be tracked for about 60 minutes. The telescope's collecting area is about 7000 m^2 (equivalent to a 94-m diameter parabolic dish). Due to the $E-W$ elongated shape of the mirrors, some of the instrument's characteristics depend on the declination at which one observes. At 21-cm wavelength the telescope's half-power beam width (HPBW) is $3\rlap{.}'5$ in right ascension, independent of declination, while in the North-South direction it is 23′ for declinations up to $\sim$20°, rising to 25′ at $\delta = 40°$ and to 33′ at $\delta = 73°$, the northern limit of the survey (see also Matthews & van Driel 2000). The instrument's effective collecting area and, consequently, its gain, follow the same geometric effect, decreasing correspondingly with declination. All observations for our project were made after a major renovation of the instrument's focal system (e.g., van Driel et al. 1997), which resulted in a typical system temperature of 35 K.

The initial observations were made in the period June – December 2002, using a total of about 350 h of telescope time. A number of follow-up observations were made to check tentative detections in late 2007 and in late 2008. We obtained our observations in total power (position-switching) mode using consecutive pairs of 40 s ON and 40 s OFF-source integrations. OFF-source integrations were taken at a position about 20′ E of the target position. Different autocorrelator modes were used for the observation of sources with previously known radial velocities and for velocity searches of objects of unknown redshift.

The autocorrelator was divided into one pair of cross-polarized receiver banks, each with 4096 channels and a 50 MHz bandpass, resulting in a channel spacing of 2.6 km s^{-1}. The centre frequencies of the 2 banks were usually tuned to 5600 km s^{-1}, for a velocity search in the $\sim$325 to 11 825 km s^{-1} range; for 8 undetected galaxies, which are flagged in Table 2, the centre frequency was tuned to 5000 km s^{-1}, resulting in a $\sim$−275 to 11 225 km s^{-1} search range.

Flux calibration, i.e., the declination-dependent conversion of observed system temperatures to flux densities in mJy, is determined for the Nançay telescope through regular measurements of a cold load calibrator and periodic monitoring of strong continuum sources by the Nançay staff. Standard calibration procedures include correction for the above-mentioned declination-dependent gain variations of the telescope (e.g., Fouqué et al. 1990). We also observed a number of calibrator galaxies throughout our observing runs, whose integrated line fluxes are on average 0.95 ± 0.25 times our values (Monnier Ragaigne et al. 2003b).

The first steps in the data reduction were made using software developed by the Nançay staff (NAPS, SIR program

packages). With this software we averaged the two receiver polarizations and converted the flux densities to mJy. Further data analysis was performed using Supermongo routines developed by one of us (SES). With these we subtracted baselines (generally third order polynomials were fitted), excluding those velocity ranges with H I line emission or radio frequency interference (RFI). Once the baselines were subtracted, the radial velocities were corrected to the heliocentric system. The central line velocity, line widths at, respectively, the 50% and 20% level of peak maximum (Lewis 1983), the integrated flux of the H I profiles, as well as the rms noise of the spectra were determined. All data were boxcar smoothed to a velocity resolution of 15.7 km s^{-1} for further analysis.

In order to reduce the effect of radio frequency interference (RFI) in our observations, we used an off-line RFI mitigation program, which is part of the standard Nançay NAPS software package, see Sect. 3.3.

3.2. Arecibo observations and data reduction

We observed a sample (see Sect. 2.2) of 81 LSB galaxies in the ZoA from a pre-release version of the 2MASS working database using the refurbished 305-m Arecibo Gregorian radio telescope in November 2000 and January 2001, for a total of about 30 h observing time. Data were taken with the L-Band Narrow receiver using nine-level sampling with two of the 2048 lag subcorrelators set to each polarization channel. All observations were taken using the position-switching technique, with the blank sky (or OFF) observation taken for the same length of time, and over the same portion of the Arecibo dish (as defined by the azimuth and zenith angles) as was used for the on-source (ON) observation. Each ON+OFF pair was followed by a 10 s ON+OFF observation of a well calibrated, uncorrelated noise diode. The observing strategy used was as follows: first, a minimum of one 3 min ON/OFF pair was taken of each galaxy, followed by a 10 s ON/OFF calibration pair. If a galaxy was not detected, one or more additional 3 min ON/OFF pairs were taken of the object, if it was deemed of sufficient interest (e.g., large diameter, known optical velocity).

The 4 subcorrelators were set to 25MHz bandpasses, and both subcorrelators with the same polarization were set to overlap by 5MHz. This allowed a wide velocity search while ensuring that the overlapping region of the two boards was adequately covered. Two different velocity searches were made – first in the velocity range –500 to 11 000 km s^{-1} and subsequently in the range 9500 to 21 000 km s^{-1} (assuming the galaxy was not detected in the lower velocity range and observing time permitting). The instrument's HPBW at 21 cm is $3'.6 \times 3'.6$ and the pointing accuracy is about 15″.

Using standard data reduction software available at Arecibo, the two polarizations were averaged, and corrections were applied for the variations in the gain and system temperature of the telescope with zenith angle and azimuth using the most recent calibration data available at the telescope. Further data analysis was performed as mentioned above for the Nançay data. A baseline of order zero was fitted to the data, excluding those velocity ranges with H I line emission or radio frequency interference. Once the baselines were subtracted, the velocities were corrected to the heliocentric system, and the central line velocity, line widths at, respectively, the 50% and 20% level of peak maximum (Lewis 1983), the integrated flux, as well as the rms noise of the spectra were determined. All data were boxcar smoothed to a velocity resolution of 14.3 km s^{-1} for analysis.

The stability of the chain of reception of the Arecibo telescope is shown by the observations we made of strong continuum sources and of a calibration galaxy with a strong line signal: the latter showed a ±6% standard deviation in its integrated line flux.

3.3. Radio frequency interference (RFI)

As a consequence of their high sensitivity, radio astronomy telescopes are vulnerable to radio frequency interference (RFI), with signal strengths usually greatly exceeding those of the weak observed celestial radio sources. Broad-band RFI raises the noise level of the observations, while narrow-band RFI may mimic spectral lines like the H I lines from galaxies that are being searched for in the present study. Besides external RFI, interference signals generated within the radio observatory, including the telescope system itself, may degrade the quality of the observations.

At Nançay, where the renovated telescope had only recently been put back into operation at the time of the observations, persistent internal RFI occurred in the 3600–3800 and 4600–4900 km s^{-1} range and external RFI often occurred around 8300, 9000 and 10 500 km s^{-1}. The external RFI can be highly variable in time, and some occur in one polarisation only.

At Arecibo an internal RFI source that wandered in frequency throughout the observed band, occurred regularly throughout the observing runs, besides the usual external RFI around 8300 and 15 000 km s^{-1}.

RFI signals with strengths that make the detection of faint H I line signals impossible in certain radial velocity ranges were present during a significant fraction of the observations, both at Nançay and at Arecibo. At Arecibo, besides a hardware radar-blanker, no software was available to identify and mitigate RFI signals. At Nançay, we used an off-line RFI mitigation program, as described in Monnier Ragaigne et al. (2003b).

4. Results

Nançay observations of the following 12 2MASX sources could not be used due to extremely high rms noise levels (>15 mJy), most likely caused by strong nearby continuum sources: 04124692+3835153, 04350092+5939419, 07392356-3221214, J08204513-3616164, 16171926-3740403, 16434955-3705384, 17504702-3116296, 18223005-0232233, 18340392-2524398, 20423202+4256315, 23044546+6004370, and 23045989+6014030. We completely exclude these objects in the following tables, plots an discussions. Apart from these sources, the Nançay rms typically ranges from about 2–4 mJy for the detections with a few outliers, whereas the non-detections spread more widely between 2 and 8 mJy (see Tables 1 and 3). For the Arecibo observations, detections and non-detections all have quite low rms, hovering narrowly around 1 mJy (see Tables 4 and 6).

Furthermore, we have not included the results for the 16 2MASS sources from versions of the working database sources that did not make it into the final 2MASS source catalogue (see Sect. 2.1), none of which were detected in H I.

The resulting data are presented in the following figures and two sets of 3 tables for the Nançay and Arecibo data. The H I spectra of the objects detected at Nançay and at Arecibo are shown in Figs. 2 and 3, respectively and the composite 2MASS JHK_s images of all detected sources are displayed in Fig. 4. The H I parameters of the detected galaxies obtained with the Nançay

Table 1. Nançay: observational data.

No	2MASX J	PGC No	Other name	K_{20}	$J-K$	$H-K$	r_{K20}	b/a	B_{T_C}	D_{25}	I_{HI}	V_{50}	W_{50}	W_{20}	rms	S_{max}
				mag	mag	mag	″		mag	′	$\frac{Jykm}{s}$	$\frac{km}{s}$	$\frac{km}{s}$	$\frac{km}{s}$	mJy	mJy
(1)	(2)	(3)	(4)	(5)	(6)	(7)	(8)	(9)	(10)	(11)	(12)	(13)	(14)	(15)	(16)	(17)
N01	00475430+6807433	137211	ZOAG 122.60+05.26	10.86	1.41	0.49	37.00	0.38	*	0.2	11.7 ± 0.6	761 ± 1	338	351	3.93	58
N02	01203021+6525055	137634	ZOAG 125.95+02.72	9.96	1.43	0.45	40.10	0.58	*	0.4	15.8 ± 0.9	4150 ± 3	419	447	5.02	80
N03	03261404+6635372	2797282	ZOAG 137.47+08.19	8.98	1.23	0.38	44.00	0.74	*	1.8	1.0 ± 0.3	5460 ± 2	101	111	3.15	20
N04	03302327+6110135	168353	ZOAG 140.93+03.98	9.39	1.49	0.43	42.90	0.56	12.12	0.7	3.0 ± 0.4	3678 ± 16	231	281	3.04	14
N05	03394709+6528486	2677859	ZOA 139.25+08.09	10.15	1.43	0.40	37.70	0.52	11.89	0.7	10.2 ± 0.9	5219 ± 1	437	446	5.02	52
N06	04212943+3656572	*	*	9.31	1.26	0.35	34.80	0.88	*	*	1.1 ± 0.3	2435 ± 5	80	102	2.36	16
N07	04244617+4244494	101333	ZOAG 159.16-04.63	10.42	1.16	0.35	43.20	0.20	11.58	1.5	3.3 ± 0.4	6018 ± 3	506	521	1.98	15
N08	04333811+4530061	15526	ZOAG 158.26-01.58	9.66	1.54	0.48	52.90	0.36	*	0.7	7.2 ± 0.4	3858 ± 3	320	339	2.48	27
N09	04464159+4943063	2798769	ZOAG 156.57+02.86	11.00	1.29	0.41	34.50	0.58	*	0.9	3.6 ± 0.5	6582 ± 3	367	381	2.83	18
N10	04514426+3856227	168835	ZOAG 165.41-03.37	10.56	1.43	0.42	38.30	0.28	*	0.9	8.2 ± 0.6	3919 ± 3	357	374	3.56	36
N11	07492337-3542214	2807067	HIZSS 25	10.69	1.64	0.46	38.20	0.68	*	0.8	15.1 ± 0.2	2863 ± 1	47	69	3.35	300
N12	08080461-1452387	79913	FGC 717	10.69	1.17	0.36	34.90	0.24	13.27	1.9	5.8 ± 0.5	6575 ± 3	463	481	2.53	22
N13	08170147-3410277	*	2MFGC 6552	10.74	1.46	0.50	39.20	0.16	*	*	9.2 ± 0.7	10373 ± 5	622	651	2.94	27
N13 S	(0816586-3420024)	*									6.4 ± 0.6	10380 ± 5	(207)	592	2.74	27
N14	08410265-3303095	24405	ESO 371-5	11.24	1.02	0.17	40.70	0.20	13.16	1.1	1.2 ± 0.3	1901 ± 16	185	240	1.99	10
[N15]	08544150-3248590	25014	ESO 371-027	*	*	*	*	(0.4)	15.46	0.6	>2.2	1302	73	98	3.04	36
N16	16183236-3723459	623805	*	9.82	1.34	0.43	39.40	0.88	*	0.3	4.5 ± 0.8	4584 ± 12	156	206	6.22	38
N17	18071027-0249517	2801967	HIPASS 1807-02	10.27	1.38	0.40	36.50	0.84	*	1.1	31.3 ± 0.1	1767 ± 1	143	165	1.27	280
N18	18153013-0253481	166531	*	9.05	1.69	0.46	69.00	0.57	*	0.3	9.2 ± 0.3	1786 ± 1	313	329	1.99	42
N19	18360975-2505397	207189	CGMW 4-1770	9.78	1.29	0.38	44.60	0.38	*	1.3	10.5 ± 0.6	6572 ± 4	608	635	2.91	33
N20	20272088+5357579	2455941	*	9.99	1.10	0.30	34.30	0.52	13.71	0.8	2.7 ± 0.3	3281 ± 2	217	228	2.02	21
N21	20572285+4808542	*	*	10.42	1.86	0.58	41.00	0.26	*	*	6.5 ± 0.7	5697 ± 7	417	441	4.04	22
N22	21135161+4255323	*	2MFGC 16082	13.16	1.28	0.23	16.5	0.28	*	*	3.9 ±	4437 ±	277	301	3.27	23
N23	23535349+5210172	72790	UGC 12836	11.35	1.05	0.24	29.80	0.34	13.34	1.0	4.7 ± 0.5	4724 ± 2	336	346	3.04	25

Notes: No. N15: galaxy ESO 371-27 was detected in the beam centred on the undetected target, ESO 371-26 (see Sect. 4.1).

Table 2. Nançay: derived data.

No.	l	b	A_B	D	k_{J-K}	R_{K20}	$\log(M_{HI})$	$\log(L_K)$	$\log(\frac{M_{HI}}{L_K})$	$\log(L_B)$	$\log(\frac{M_{HI}}{L_B})$	v_{rot}	$\log(M_{dyn})$	$\log(\frac{M_{baryon}}{M_{dyn}})$
	deg	deg	mag	Mpc	mag	kpc	$M_\odot$	$L_{\odot,K}$		$L_{\odot,B}$		$\frac{km}{s}$	$M_\odot$	
(1)	(2)	(3)	(4)	(5)	(6)	(7)	(8)	(9)	(10)	(11)	(12)	(13)	(14)	(15)
N01	122.60	5.26	5.01	15.0	0.01	2.7	8.79	9.50	−0.71	*	*	182.7	10.32	−0.79
N02	125.95	2.72	5.58	60.9	0.04	11.8	10.14	11.10	−0.96	*	*	257.2	11.26	−0.18
N03	137.46	8.19	4.02	78.0	0.05	16.6	9.17	11.65	−2.48	*	*	75.1	10.33	1.23
N04	140.93	3.98	4.21	52.6	0.03	10.9	9.29	11.15	−1.86	10.79	−1.50	139.4	10.69	0.38
N05	139.25	8.00	4.37	74.4	0.04	13.6	10.12	11.16	−1.03	11.18	−1.06	255.8	11.31	−0.18
N06	162.89	−9.13	4.14	34.3	0.02	5.8	8.47	10.81	−2.34	*	*	84.2	9.97	0.75
N07	159.16	−4.63	2.62	84.3	0.05	17.7	9.74	11.10	−1.35	11.41	−1.67	258.2	11.43	−0.39
N08	158.25	−1.58	5.62	53.2	0.03	13.6	9.68	11.10	−1.42	*	*	171.5	10.97	0.06
N09	156.56	2.86	3.85	92.4	0.05	15.5	9.87	10.99	−1.12	*	*	225.2	11.26	−0.31
N10	165.41	−3.37	4.22	53.3	0.03	9.9	9.74	10.70	−0.96	*	*	185.9	10.90	−0.22
N11	250.83	−4.89	6.11	41.1	0.02	7.6	9.78	10.48	−0.70	*	*	32.0	9.26	1.26
N12	235.16	9.51	0.30	92.7	0.05	15.7	10.07	10.99	−0.92	10.82	−0.75	238.5	11.31	−0.33
N13	252.54	0.72	2.07	147.9	0.09	28.1	10.68	11.44	−0.76	*	*	315.0	11.81	−0.35
N14	254.56	5.43	1.28	23.9	0.01	4.7	8.23	9.63	−1.40	9.68	−1.45	94.4	9.98	−0.41
[N15]	256.17	7.82	1.36	14.3	0.01	*	8.37	*	*	8.32	0.05	*	*	*
N16	342.15	9.24	5.34	63.5	0.04	12.1	9.64	11.18	−1.55	*	*	164.2	10.88	0.23
N17	25.30	8.52	6.91	23.6	0.01	4.2	9.62	10.20	−0.58	*	*	131.8	10.22	0.05
N18	26.22	6.64	9.43	23.9	0.01	8.0	9.09	10.78	−1.69	*	*	190.5	10.82	−0.12
N19	8.79	−8.03	1.81	90.3	0.05	19.5	10.31	11.39	−1.08	*	*	328.6	11.69	−0.33
N20	89.96	8.97	1.47	49.4	0.03	8.2	9.20	10.77	−1.57	10.10	−0.90	127.0	10.48	0.22
N21	88.24	1.69	10.79	83.1	0.05	16.5	10.03	11.36	−1.34	*	*	215.9	11.25	0.05
N22	86.29	−3.95	3.64	65.5	0.04	5.2	9.60	9.82	−0.22	*	*	144.3	10.40	−0.36
N23	114.04	−9.70	1.64	70.3	0.04	10.2	9.74	10.53	−0.79	10.55	−0.81	178.6	10.87	−0.33

Notes: No. N15: galaxy ESO 371-27 was detected in the beam centred on the undetected target, ESO 371-26 (see Sect. 4.1).

and Arecibo instruments are given in Table 1 and Table 4, respectively, including the main 2MASS parameters, and where available also the optical magnitudes and diameters. The latter were taken from the HyperLeda database (Paturel et al. 2003a), or retrieved from NED (then noted in parentheses). This is followed by Tables 2 and 5 which give the derived global properties of the galaxies. The non-detections are listed in Tables 3 and 6 with their main 2MASS parameters, Galactic extinction A_B, and H I rms noise levels.

Table 4. Arecibo: observational data.

No	2MASX J	PGC No	Other name	K_{20}	$J-K$	$H-K$	r_{K20}	b/a	B_{T_c}	D_{25}	I_{HI}	V_{50}	W_{50}	W_{20}	rms	S_{max}
				mag	mag	mag	$''$		mag	$'$	$\frac{\text{Jykm}}{\text{s}}$	$\frac{\text{km}}{\text{s}}$	$\frac{\text{km}}{\text{s}}$	$\frac{\text{km}}{\text{s}}$	mJy	mJy
(1)	(2)	(3)	(4)	(5)	(6)	(7)	(8)	(9)	(10)	(11)	(12)	(13)	(14)	(15)	(16)	(17)
A01	04545536+3454433	143 016	CAP 0451+34	12.32	1.46	0.48	19.80	0.34	14.76	0.71	6.1 ± 0.3	$11\,433 \pm 4$	434	469	1.94	26
A02	05005348+3436115	*	*	12.31	1.43	0.45	15.50	0.66	*	*	2.7 ± 0.2	15352 ± 2	250	266	1.51	18
A03	05103476+2838002	1841450	*	13.31	1.37	0.44	6.10	0.80	15.69	0.32	1.3 ± 0.2	17301 ± 11	288	333	1.00	6
A04	05112278+3621199	*	*	13.87	1.43	0.71	8.70	0.39	*	*	0.56 ± 0.13	7861 ± 8	191	220	1.04	6
A05	05165184+2919457	*	2MFGC 4312	13.09	1.17	0.59	10.80	0.30	15.10	0.35	0.32 ± 0.11	14414 ± 10	128	155	1.03	4
A06	05183772+3502015	*	*	12.52	1.51	0.49	14.70	0.46	*	*	1.0 ± 0.2	9008 ± 3	338	350	1.18	7
A07	05214377+1923370	1590726	*	13.78	0.96	0.24	10.40	0.46	15.68	0.62	2.3 ± 0.1	4360 ± 2	203	217	1.08	15
A08	05315137+1517480	3097140	*	11.75	1.16	0.34	23.10	0.46	*	*	2.6 ± 0.1	5812 ± 2	180	206	1.14	20
A09	05384324+1616012	*	*	12.35	1.03	0.22	16.00	0.46	*	*	1.5 ± 0.2	5284 ± 2	262	273	1.27	9
A10	05393262+3031377	*	*	13.01	1.48	0.64	9.50	0.66	*	*	1.7 ± 0.1	9384 ± 2	114	137	1.01	20
A11	05420143+1856156	*	*	13.50	1.28	0.44	6.30	0.80	*	*	1.3 ± 0.2	7603 ± 64	216	414	1.08	5
A12	05422061+2448359	*	IRAS 05393+2447	13.38	1.87	0.88	12.20	0.39	*	*	0.79 ± 0.10	529 ± 18	95	179	0.88	6
A13	05453428+1307035	1423303	2MFGC 4668	12.60	1.11	0.32	20.60	0.30	15.28	0.51	3.5 ± 0.1	7325 ± 4	279	331	0.86	15
A14	05490625+1904314	136129	ZOAG 188.86-04.41	12.09	1.19	0.35	21.60	0.30	*	0.40	1.5 ± 0.1	5782 ± 3	312	327	0.85	7
A15	05594377+3224327	*	2MFGC 4834	11.93	1.49	0.43	30.40	0.14	*	*	1.7 ± 0.1	7765 ± 2	398	412	0.81	8
A16	05595654+2850437	1847776	*	12.94	1.25	0.38	10.60	0.56	15.97	0.36	0.7 ± 0.1	9406 ± 29	259	365	0.88	5
A17	06001509+1537007	136218	ZOAG 193.20-03.85	12.32	1.11	0.31	19.40	0.32	*	0.98	0.56 ± 0.09	5459 ± 5	206	272	0.64	14
A18	06023193+2833375	136013	ZOAG 182.20+03.01	13.01	1.29	0.42	13.10	0.32	16.25	0.31	1.4 ± 0.1	8584 ± 11	101	166	1.01	9
A19	06062918+2623371	136075	ZOAG 184.52+02.71	14.20	1.07	0.27	10.30	0.24	13.44	1.03	4.0 ± 0.1	2715 ± 1	205	229	1.04	26
A20	06103483+2602595	136084	ZOAG 185.27+03.35	12.27	1.29	0.44	18.50	0.30	15.95	0.40	1.3 ± 0.2	9398 ± 11	323	361	1.19	6
A21	06181671+2911295	143067	CAP 0615+29a	12.20	1.17	0.41	15.50	0.74	15.21	0.48	1.2 ± 0.2	10538 ± 8	293	323	1.19	7
A22	06242643+2213057	*	*	13.40	1.36	0.56	9.40	0.68	*	*	0.75 ± 0.07	1404 ± 16	50	101	0.86	4
A23	06261975+2320174	143077	*	11.89	1.11	0.27	20.10	0.44	14.32	0.81	2.4 ± 0.1	4547 ± 2	230	251	0.75	14
A24	06301575+1646422	136308	ZOAG 195.62+03.04	11.67	1.10	0.32	20.20	0.42	14.71	0.59	10.5 ± 0.1	2525 ± 1	267	285	0.81	55
A25	06385063+1155111	136449	ZOAG 200.89+02.66	12.77	1.36	0.46	12.60	0.40	15.37	0.32	2.1 ± 0.2	7536 ± 3	294	312	1.15	11
A26	07032646+1249080	1416812	*	12.53	1.00	0.34	14.80	0.40	15.67	0.63	1.1	7931 ± 3	304	315	0.91	5
A27	07055211+1451243	1468922	*	13.04	1.05	0.32	10.80	0.52	16.08	0.59	2.6 ± 0.2	4623 ± 2	222	241	0.91	17
A28	20114449+1526113	*	*	12.30	1.04	0.34	15.40	0.44	*	*	1.2 ± 0.1	6352 ± 8	276	316	0.66	5
A29	20312562+2258155	1679168	2MFGC 15573	13.40	1.46	0.46	11.80	0.30	17.53	0.52	1.4 ± 0.1	8237 ± 3	289	307	0.88	7

The 2MASS data for these sources have all been updated to the final release values. In a number of cases the working database values differed significantly, particularly because ellipse fits to galaxies can be quite unstable in the presence of multiple confusing foreground stars.

The global H I line parameters listed in the tables are directly measured values; no corrections have been applied to them for, e.g., instrumental resolution. Uncertainties $\sigma_{V_{HI}}$ in V_{HI} and $\sigma_{I_{HI}}$ in I_{HI} can be determined following Schneider et al. (1986, 1990), as, respectively

$$\sigma_{V_{HI}} = 1.5(W_{20} - W_{50})X^{-1} \ (\text{km s}^{-1}) \quad (1)$$

$$\sigma_{I_{HI}} = 2(1.2W_{20}R)^{0.5}\sigma \ (\text{km s}^{-1}) \quad (2)$$

where R is the instrumental resolution in km s^{-1} (see Sect. 3), X is the signal-to-noise ratio of a spectrum, which we define as the ratio of the peak flux density S_{max} and the rms dispersion in the baseline, σ (both in Jy). Following Schneider et al., the uncertainty in the W_{20} and W_{50} line widths is expected to be 2 and 3.1 times $\sigma_{V_{HI}}$.

*Description of all parameters listed in the tables, in alphabetical order:*

(1) *2MASX J* is the entry number of a source in the final 2MASS Extended Source Catalog, corresponding to the right ascension and declination of the source centre in (J2000.0) coordinates;

(2) A_B is the Galactic B-band extinction in this direction in the Milky Way as estimated by Schlegel et al. (1998);

(3) b/a is the infrared axis ratio determined from an ellipse fit to the co-addition of the J-, H-, and K_s-band images;

(4) B_{T_c} is the total apparent B-band magnitude reduced to the RC3 system (de Vaucouleurs et al. 1991) and corrected for Galactic extinction, inclination and redshift effects (see Paturel et al. 1997, and references therein);

(5) $D = V_0/H_0$ is the galaxy's distance (in Mpc), where V_0 is its radial velocity (in km s^{-1}) corrected to the Galactic Standard of Rest and for infall towards various galaxy clusters in the local Universe, following Tonry et al. (2000), and a Hubble constant $H_0 = 75$ km s^{-1} Mpc^{-1};

(6) D_{25} is the diameter (in arcmin) at a visual surface brightness of approximately 25 mag arcsec^{-2};

(7) I_{HI} is the integrated line flux (in Jy km s^{-1});

(8) $H - K$ and $J - K$ are the infrared colours within the r_{K20} isophotal aperture. Note that these colours are not corrected for extinction, hence reddened depending on the foreground dust column density by the amounts of $f_{H-K} = 0.05A_B$ for $H-K$ and $f_{J-K} = 0.12A_B$ for $J-K$ respectively;

(9) K_{20} is the total K_s-band magnitude measured within the r_{K20} isophotal aperture;

(10) k_{J-K} is the k-correction to the $J - K$ colour;

(11) l and b are, respectively, the Galactic longitude and latitude of the source centre (in degrees);

(12) L_B is the B-band luminosity corrected for Galactic and internal extinction in solar units, for an assumed solar absolute magnitude of $5^m.48$ (Allen 1973);

(13) L_K is the K_s band luminosity of the galaxy in solar luminosities within the r_{K20} isophotal aperture, for an assumed solar absolute magnitude of $3^m.31$ (Colina & Bohlin 1997);

(14) $\frac{M_{baryon}}{M_{dyn}}$ is the ratio of the combined H I and stellar baryonic mass as a fraction of the total dynamical mass, where $M_{baryon} = 0.8L_K + 1.4M_{HI}$ (McGaugh et al. 2000 or 2003);

(15) M_{dyn} is the dynamical mass (in $M_\odot$) estimated from the rotation speed and the K_s-band radius, $M_{dyn} = v_{rot}^2 r_{K20}/G$;
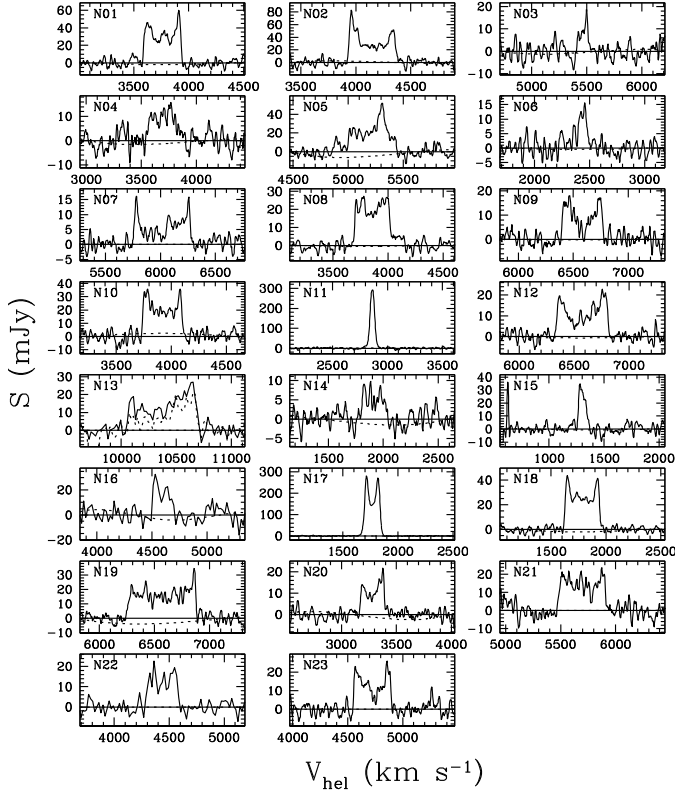
Fig. 2. Nançay 21-cm H I line spectra of the detected galaxies (see Table 1). Velocity resolution is 15.7 km s^{-1}. For object N13 two spectra are shown – the solid line represents the data taken in the direction of the target source, whereas the dashed line shows the data taken towards the galaxy 10′ South of it (see Sect. 4.3). For object N15, the spurious detection is actually of the galaxy ESO 371-27 which lies in the beam centred on the undetected target, ESO 371-26 (see Sect. 4.1).
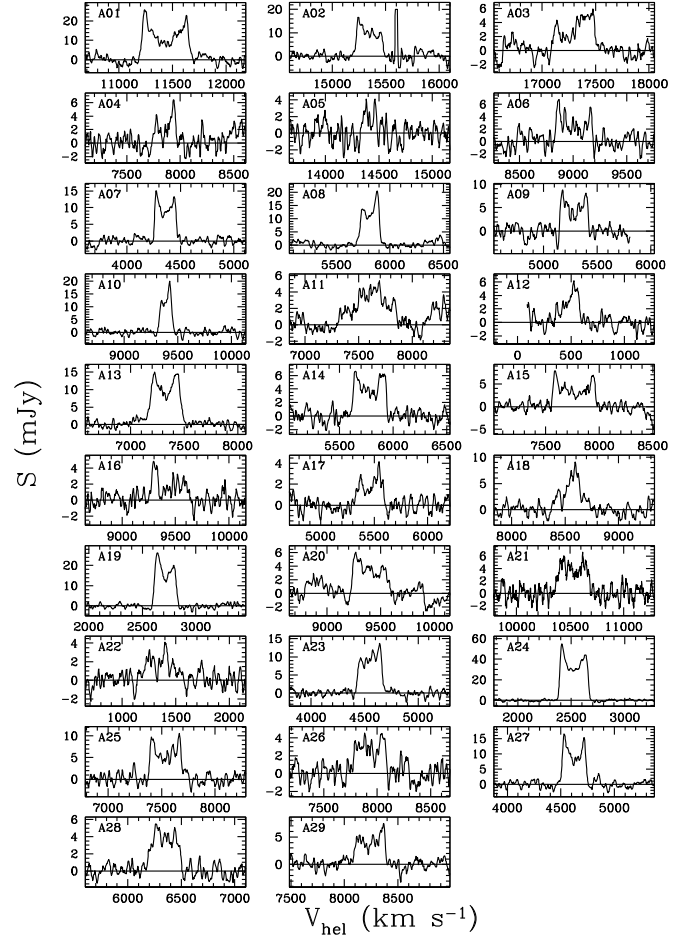
Fig. 3. Arecibo 21-cm H I line spectra of detected galaxies (see Table 4). Velocity resolution is 14.3 km s^{-1}.

(16) M_{HI} is the total H I mass (in $M_\odot$), $M_{\mathrm{HI}} = 2.356\ 10^5 D^2\ I_{\mathrm{HI}}$;

(17) M_{HI}/L_K is the ratio of the total H I mass to the K_{s}-band luminosity in solar units;

(18) *No* gives the source number used in Figs. 2–4;

(19) *Other Name* is the entry number in another major galaxy catalogue;

(20) *PGC No* is the entry number in the Principal Galaxy Catalogue (Paturel et al. 1989);

(21) $r_{K_{20}}$ is the radius (in arcsec) at a surface brightness of 20 mag arcsec^{-2} in the K_{s} band (in arcsec in Tables 1 and 4, in kpc in Tables 2 and 5);

(22) rms is the rms noise level or σ in the H I spectrum (in mJy) – if two numbers are given, the first is for the low-velocity search and the second for the high-velocity one (see Sect. 2.2);

(23) $S_{\max}$ is the peak flux density of the line (in mJy);

(24) V_{50} is the heliocentric central radial velocity of a line profile (in km s^{-1}), in the optical convention, taken as the average of the high and low velocity edges of the H I profile, measured at 50% of peak flux density;

(25) v_{rot} is the rotation speed corrected for inclination i; $v_{\mathrm{rot}} = W_{50}/2\sin(i)$ for $\sin(i) < 0.2$, for galaxies with higher inclinations we assumed $v_{\mathrm{rot}} = W_{50}/2$;

(26) W_{50} and W_{20} are the profile's velocity widths (in km s^{-1}) at 50% and 20% of peak maximum, respectively.

4.1. Comparison with published H I data

In the literature we found the following 10 H I detections of sources we observed (see also Sect. 4.1 and Table 7): 4 made at Arecibo (A01, A19, A21 and A23), 1 at Effelsberg (N12), 1 at Nançay (N10), and 4 at Parkes (A24, N11, N17 and N18). Excluding the Effelsberg data for N12, which are affected by RFI, and the Parkes data for A24, which appears to have been resolved by the Arecibo beam, we find a good overall agreement between the global profile parameters measured by us and taken from the literature: the mean of the absolute values of the differences is 7 ± 8 km s^{-1} in V_{HI} and 7 ± 6 km s^{-1} in W_{50}, and our I_{HI} fluxes are on average 1.0 ± 0.2 times the literature values.

4.2. Notes on individual galaxies

In order to identify galaxies within the telescope beams that might give rise to confusion with the H I profile of the target galaxy, we inspected 2MASS and DSS images centred on the position of each clearly or marginally detected source, over an area of $12' \times 36'$ and $8' \times 8'$ ($\alpha \times \delta$) for the Nançay and Arecibo data, respectively, and queried the NED and HyperLeda databases for information on objects in these areas – the results for objects whose data are likely to be confused are put in brackets in the tables. The data listed below were preferentially taken from the mean values listed in HyperLeda, unless otherwise indicated.

Table 5. Arecibo: derived data.

No.	l	b	A_B	D	k_{J-K}	R_{K20}	$\log(M_{HI})$	$\log(L_K)$	$\log\left(\frac{M_{HI}}{L_K}\right)$	$\log(L_B)$	$\log\left(\frac{M_{HI}}{L_B}\right)$	v_{rot}	$\log(M_{dyn})$	$\log\left(\frac{M_{baryon}}{M_{dyn}}\right)$
	deg	deg	mag	Mpc	mag	kpc	$M_\odot$	$L_{\odot,K}$		$L_{\odot,B}$		$\frac{km}{s}$	$M_\odot$	
(1)	(2)	(3)	(4)	(5)	(6)	(7)	(8)	(9)	(10)	(11)	(12)	(13)	(14)	(15)
A01	168.95	−5.41	3.97	163.8	0.10	15.7	10.58	10.96	−0.37	10.72	−0.14	230.7	11.28	−0.18
A02	169.95	−4.64	3.47	220.0	0.13	16.5	10.49	11.20	−0.72	*	*	166.4	11.02	0.21
A03	176.00	−6.56	3.34	247.8	0.14	7.3	10.28	10.90	−0.62	10.70	−0.42	240.0	10.99	−0.03
A04	169.84	−1.88	4.40	110.8	0.06	4.7	9.21	10.02	−0.80	*	*	103.7	10.06	−0.03
A05	176.23	−5.04	2.65	206.5	0.12	10.8	9.51	10.81	−1.30	10.78	−1.27	67.1	10.05	0.70
A06	171.77	−1.45	4.38	127.9	0.07	9.1	9.60	10.68	−1.08	*	*	190.3	10.88	−0.23
A07	185.14	−9.72	1.86	58.6	0.03	3.0	9.26	9.41	−0.15	9.46	−0.20	114.3	9.95	−0.29
A08	189.96	−9.89	2.87	79.5	0.05	8.9	9.60	10.52	−0.93	*	*	101.4	10.32	0.19
A09	190.00	−7.98	2.16	71.5	0.04	5.5	9.25	10.17	−0.92	*	*	147.5	10.44	−0.28
A10	177.95	−0.28	5.24	133.3	0.08	6.1	9.86	10.55	−0.69	*	*	75.9	9.91	0.68
A11	188.12	−5.92	1.87	106.4	0.06	3.3	9.53	10.04	−0.51	*	*	180.0	10.38	−0.25
A12	183.14	−2.78	4.42	8.8	0.01	0.5	7.16	8.01	−0.85	*	*	51.6	8.50	−0.49
A13	193.59	−8.18	2.28	102.3	0.06	10.2	9.94	10.38	−0.44	10.10	−0.16	146.2	10.70	−0.20
A14	188.86	−4.41	3.19	78.6	0.05	8.2	9.34	10.39	−1.05	*	*	163.5	10.70	−0.34
A15	178.55	4.38	3.06	108.7	0.06	16.0	9.69	10.73	−1.04	*	*	201.0	11.17	−0.47
A16	181.67	2.65	2.10	133.4	0.08	6.9	9.49	10.47	−0.98	10.05	−0.56	156.3	10.59	−0.14
A17	193.20	−3.85	2.38	73.7	0.04	6.9	8.86	10.21	−1.36	*	*	108.7	10.27	−0.12
A18	182.20	3.01	1.80	121.0	0.07	7.7	9.68	10.35	−0.66	9.86	−0.18	53.3	9.70	0.69
A19	184.52	2.71	2.15	35.7	0.02	1.8	9.08	8.82	0.26	9.92	−0.84	105.6	9.66	−0.31
A20	185.27	3.35	2.44	133.2	0.08	11.9	9.75	10.75	−1.00	10.06	−0.31	169.3	10.90	−0.17
A21	183.30	6.34	2.49	150.0	0.09	11.3	9.81	10.88	−1.07	10.46	−0.65	217.8	11.09	−0.24
A22	190.15	4.34	2.63	19.1	0.01	0.9	7.81	8.62	−0.81	*	*	34.1	8.37	0.26
A23	189.35	5.24	1.82	60.0	0.04	5.8	9.32	10.19	−0.87	10.02	−0.70	128.1	10.34	−0.15
A24	195.62	3.04	2.39	33.1	0.02	3.2	9.43	9.78	−0.34	9.35	0.08	147.1	10.21	−0.27
A25	200.89	2.66	2.58	104.8	0.06	6.4	9.74	10.34	−0.60	10.09	−0.35	160.4	10.58	−0.18
A26	202.79	8.43	0.34	110.7	0.06	7.9	9.49	10.41	−0.93	10.01	−0.52	165.8	10.70	−0.30
A27	201.19	9.85	0.39	61.2	0.04	3.2	9.36	9.69	−0.34	9.33	0.03	129.9	10.10	−0.24
A28	56.12	−9.97	0.96	90.0	0.05	6.7	9.36	10.34	−0.98	*	*	153.7	10.56	−0.24
A29	65.10	−9.69	0.88	118.2	0.07	6.8	9.66	10.14	−0.47	9.33	0.33	151.5	10.55	−0.31

2MASX J04212943+3656572 (=N06): it appears also to have been detected at Nançay by Theureau et al. (1998) while pointing towards the nearby galaxy NGC 3016, which lies on the Nançay HPBW edge. NGC 3016 has a much higher redshift of 5900 km s^{-1} (Pantoja et al. 1997; Huchra et al. 1983). The galaxy NGC 3019, which also lies on the Nançay HPBW edge, has a similarly high redshift of 5664 km s^{-1} (Fisher et al. 1995; Pantoja et al. 1997; Takata et al. 1994; Theureau et al. 1998).

2MASX J04215207+3607373 (=UGC 3021): classified as an elliptical galaxy, and therefore not expected to be gas-rich. Its optical velocity is 6238 ± 60 km s^{-1} (Huchra et al. 1983). It was not detected by us at Nançay with an rms of 2.8 mJy, nor at Arecibo by Pantoja et al. (1997), whose mean rms is 1.3 mJy. It has a possible companion superimposed on it, hence the two PGC entries.

2MASX J04514426+3856227 (=N10): its optical redshift of 3913 ± 60 km s^{-1} (Saunders et al. 2000) is in agreement with our Nançay detection and that of Paturel et al. (2003b).

2MASX J05315137+1517480 (=A08): an optical velocity of 5000 ± 60 km s^{-1} (Tully 2002, private communication) was listed in Hyperleda after our Arecibo detection was made at 5812 km s^{-1}.

2MASX J06301575+1646422 (=A24): detected in H I at Parkes as HIZOA J0630+16 (Donley et al. 2005) with a three times higher line flux than our Arecibo detection. This indicates that the source has a quite extended LSB disc, which has to be much larger than its ~1′ extent on the composite 2MASS JHK_s-band image, given the respective Arecibo and Parkes HPBW of 3′.6 and 14′.4.

2MASX J07300453-1833166: this source appears to be part of a Galactic H II region, together with other nearby 2MASS sources and object ESO559-N015.

2MASX J08080461-1452387 (=N12): detected in H I at Effelsberg by Huchtmeier et al. (2005) at 6679 km s^{-1}, which is significantly higher than our value of 6575 km s^{-1}. The published spectrum shows a narrow peak at 7050 km s^{-1}, however, which does not occur in our spectrum and thus appears due to RFI. We re-estimate the Effelsberg profile parameters as listed in Table 7, which are in agreement with ours.

08544150-3248590 (near N15; =ESO 371-27): after our Nançay detection was made at 1302 km s^{-1} (consistent with the Nançay spectrum of Chamaraux et al. 1999, taking into account beam attenuation) an optical redshift of 2198 km s^{-1} was published (Wegner et al. 2003), which shows that we actually detected another galaxy within the beam, ESO 371-27, which was also detected at Parkes (Doyle et al. 2005). All H I redshifts of ESO 371-27 are consistent with the optical value of 1313 km s^{-1} (Karachentseva & Karachentsev 2000). As the Parkes line flux is significantly higher we have used it for calculating the total H I mass. The detected galaxy is very LSB and it does not have an entry in the 2MASS catalogue.

2MASX J18153013-0253481 (=N18): Inspecting the on-line Parkes H I spectrum of HIPASS J1815-02 (Meyer et al. 2004) we found that the HIPASS redshift of 1664 km s^{-1} listed in NED is actually that of one of the profile's two peaks; the correct value is 1788 km s^{-1}.

2MASX J21135161+4255323 (=N22): Although the targeted source (21135100+4257568) did not make it into the final 2MASS catalogue we made a clear detection towards this
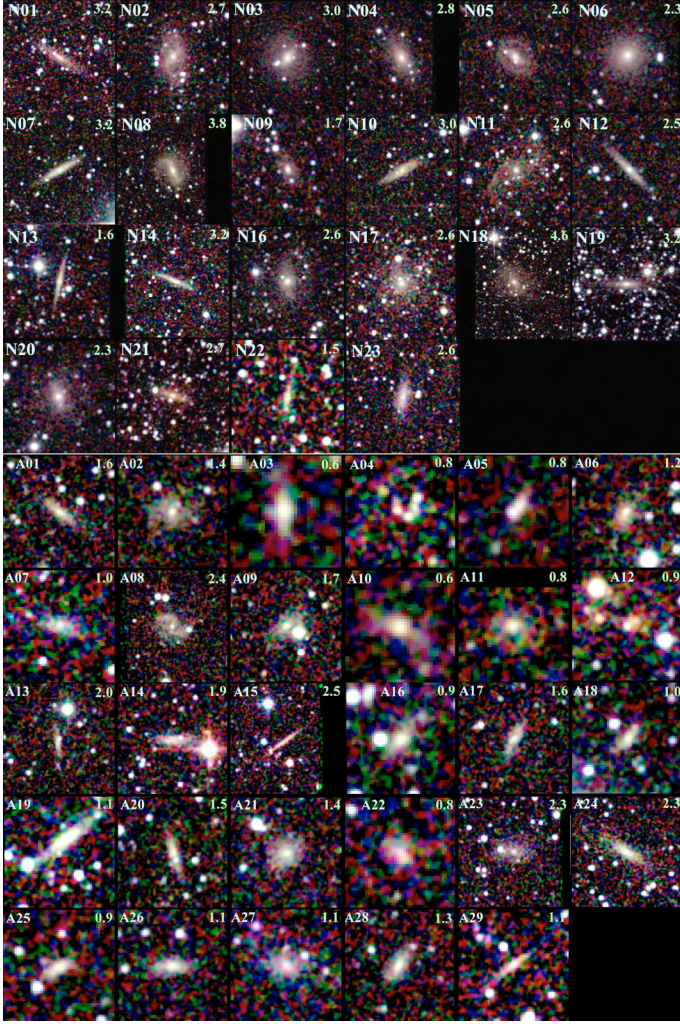
Fig. 4. Composite 2MASS composite *JHK*$_s$-band colour images of the ZoA galaxies detected in the H I line at Nançay (*top panel*) and at Arecibo (*lower panel*). The galaxy identifications (see Tables 1 and 4) are indicated in *the top-left corner* of each image and the image size in arcmin in *the top-right corner*.

position at Nançay. We have assumed this to be of 2MASX J21135161+4255323, located 1.'3 towards the south.

4.3. Unusual galaxies

2MASX J05422061+2448359 (=A12): Curiously, the galaxy that is nearest (v = 521 km s^{-1}) and lowest in H I mass (log M_{HI} = 7.16), is also the reddest in our sample. Even after correcting for the reddening of the source (A_B = 4.42), the extinction-corrected $(J - K)^o$ colour (1^{m}32) is more likely that of an extremely old elliptical than a small H I-rich dwarf. It is possible that the extinction in this direction is substantially larger than estimated by Schlegel et al. (1998). If the reddening were large enough, however, to give this object a more-typical $(J - K)^o$ colour, the extinction correction would imply an extremely large stellar mass.

Another obvious possibility is confusion with a red star. Apart from the entry in 2MASX, the 2MASS point source catalogue lists two very nearby stars at 1″ and 5″ distance respectively, where the nearer stellar counterpart might be one and the same object. The source centred on the targeted 2MASS position actually looks more like a point source with more

typical colours of a star (strong in *H*), whereas the slightly more offset 2MASS source looks more like a fuzzy reddened galaxy candidate (see Fig. 4; slightly to the NW of the central source: 2MASS 05422020+24483880). In either case the colour of the extended object will be substantially contaminated by the nearby star.

A third possibility is that neither of these objects is the counterpart of what must be a highly obscured late-type spiral galaxy (narrow Gaussian profile, low H I mass), but that the H I detection originates from the nearby completely obscured infrared source IRAS 05393+2447 – or even some other invisible galaxy.

2MASX J08170147-3410277 (=N13): This thin edge-on spiral galaxy has a radial velocity (10 369 km s^{-1}), H I mass (4.6 × 10^{10} $M_\odot$), and inclination-corrected rotation velocity (314 km s^{-1}) similar to that of the very H I-massive disc galaxy HIZOAJ0836-43, discovered by Donley et al. (2006, V = 10 689 km s^{-1}, M_{HI} = 7.5 × 10^{10} $M_\odot$, and v_{rot} = 305 km s^{-1}). The latter has about twice the estimated total dynamical mass of N13 (1.4 vs. 0.6 × 10^{12} $M_\odot$), comparable to that of the most massive known disc galaxies such as giant LSB galaxy Malin 1. It is, however, a NIR luminous star-bursting galaxy (Cluver et al. 2008) with quite distinct properties from giant LSBs.

Because such high H I mass galaxies are (a) extremely rare (they are only being formed now and their properties poorly known) *and* (b) our clear Nançay detection with a 9σ peak flux density of 27 mJy could not be found back in the deep Parkes ZoA survey data cube ZOA252 (http://www.atnf. csiro.au/research/multibeam/release/), we looked at this galaxy and detection in further detail. We first looked for possible companions which might have contributed to the broad signal by inspecting all bands of the digitized sky survey within the Nançay beam as the extinction is relatively low (A_B ∼ 2 mag). We found a previously uncatalogued galaxy of similar surface brightness about 10′ south of the target, at α = 08^{h}16^{m}58.'6, δ = −34°20′0.''24. It appears on the *B*, *R* as well as the *IR* images as a smaller (roughly half an arc minute in diameter) face-on spiral with a smallish bulge.

With an angular N-S separation of 10′ corresponding to 0.45 times the instrument's HPBW, observations towards both objects allow us in principle to disentangle their H I profiles, if their angular diameters are sufficiently small. We therefore (re)-observed both the sources N13 North and N13 South, to a similar low noise levels (see Fig. 2). The velocity range and central velocity of both profiles are the same, whereas the profile towards the southern object has 76% of the H I mass measured towards the northern one and its H I is mainly concentrated in the high-velocity peak of the double horned profile. This appears to indicate the presence of a single, relatively large source towards N13 North whose receding half is towards the south.

We attempted to reconstruct the spectra of the hypothetical H I sources N13 north and south, assuming that their sizes are significantly smaller than the telescope beam. As they are separated by about half a HPBW, this would imply that an observed spectrum is due to the target plus half of the emission of the other galaxy. This exercise showed that N13 South is not a significant source of H I in itself.

Whereas our provisional conclusion is that N13 appears to be an extended, very massive H I galaxy, it is clear that only ATCA imaging observations will allow a firm conclusion whether it has a very extended lopsided H I disc and belongs to the class of extremely massive spiral galaxies.
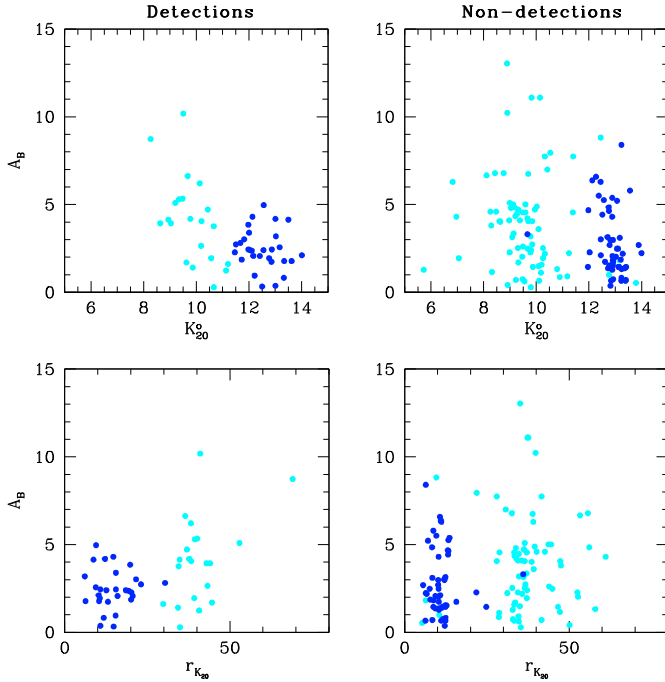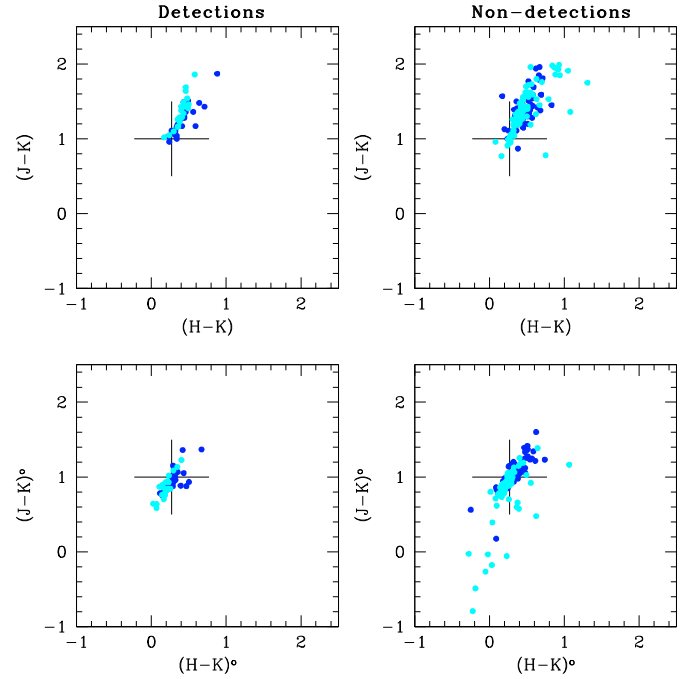
Fig. 5. Plots of the extinction-corrected total K_s-band magnitude, K_{20}^0, and the $r_{K_{20}}$ isophotal aperture as function of the galactic extinction A_B. *The two left-hand panels* show the H I detections, the two right-hand ones the non-detections. Objects observed at Nançay are shown in light blue and those observed at Arecibo in dark blue. H I detections are shown in *the two left-hand panels*, non-detections on the right. The crosses mark typical 2MASS galaxy colours (Jarrett 2003).

Fig. 6. Plots of the observed (*top*) and extinction-corrected (*bottom*) colours $(J - K)$ versus $(H - K)$, for detections (*left panels*) and non-detections (*right panels*). Objects observed at Nançay are shown in light blue and those observed at Arecibo in dark blue.

5. Discussion

5.1. Detection rate

The detection rate is quite low. Excluding the 16 working database sources that did not make it into the final 2MASS extended source catalog (Sect. 2.1), only 22 of the 116 observed sources (19%) were detected at Nançay, excluding the detections of spurious, untargeted galaxy in the beams of N15 and N22. This value is only a bit higher (21%) if we exclude the 12 strongly continuum perturbed spectra (Sect. 4) – generally a problem at very low latitudes. The on average 3.5 times higher sensitivity Arecibo observations resulted in a detection rate of 36% (29/81), only 1.9 times higher (36/19) than that at Nançay. Criteria for improving the selection of likely 2MASX candidate ZoA galaxies are discussed in Sect. 5.2 and 6.

There are various reasons – partly different for the Nançay and Arecibo observations – for the low detection rate. For both samples, no morphological type criterion was introduced when selecting the target objects, i.e. the sample includes both red gas-poor galaxies as well as blue gas-rich ones. Being NIR selected, the bias against the more blueish gas-rich galaxies is quite strong, stronger than, for instance, for optical selected samples. This bias is even more extreme for the relatively shallow and low-resolution 2MASS survey (as discussed in Sect. 1), which is hardly sensitive to LSB galaxies. It is exacerbated for ZoA galaxy candidates because of the increasing loss of low-surface brightness features *and* the selective reddening, which results in an even stronger bias towards redder, higher surface brightness early type galaxies or bulges of spirals. Given that optical spectroscopy of these optically heavily or completely obscured 2MASS galaxies is hardly possible, it should be noted that

despite this relatively low detection rate, H I observations of galaxy candidates still remain the most efficient tool in mapping large-scale structures across the ZoA.

Some of the properties of the two galaxy samples (Nançay and Arecibo) and the differences between them, as well as between detections and non-detections are apparent from Fig. 5 which shows plots of the extinction-corrected K_{20}^0 magnitude versus optical extinction A_B (top panel) and of radius (at $r_{K_{20}}$) versus A_B (bottom panel) for both detections (left panels) and non-detections (right panels). The Nançay sample is indicated in light blue and the Arecibo one in dark blue.

It is obvious that the Arecibo galaxy sample contains a fainter subset of galaxies compared to the Nançay sample, i.e. roughly ranging from 12–14 mag compared to 6–11 mag, as well as smaller galaxies (≲30″ versus ≳30″). This is due to the fact that many of the larger galaxies in the low extinction Arecibo area were already identified optically and observed with Arecibo by Pantoja et al. (1994, 1997). Although the Nançay galaxies are considerably brighter (both observed and extinction-corrected), they are traced deeper into the Galactic dust layer. The lower detection rate of the brighter Nançay galaxies is purely the result of the lower sensitivity.

Overall there seems no marked difference between the locus of points for detections and non-detections, substantiating once more that H I observations are unaffected by dust-extinction. However, two trends seem to stand out: for extinction values A_B above about 5 mag all 2MASX Arecibo sources are undetected. This implies that these apparently small, highly obscured non-detections must be very distant early-type galaxies.

Secondly, it seems surprising that none of the brightest Nançay objects (extinction-corrected) were detected. This must be due to confusion in 2MASX with Galactic sources or mis-classification of galaxies due to blending of sources. To verify

this claim, and learn from this pilot project, we investigated the brightest sources individually.

The two brightest sources ($K_{20}^o = 1^m.82, 5^m.72$; of which the brighter lies beyond the boundaries of Fig. 5) are globular clusters with the first one having colours inconsistent with a galaxy (see also Fig. 6 in the next section) and the second being borderline. But the globular cluster morphology is obvious enough in all optical and NIR wavebands.

The 3rd galaxy in the list of decreasing extinction-corrected brightness K_{20}^o (with $6^m.82$) is also an unlikely galaxy. It has the extreme colour of $(H - K^o) = 4^m.34, (J - K)^o = 0^m.27$, and is clearly heavily contaminated, in particularly in the H-band, by a bright nearby star. The remaining feature does not look like a galaxy candidate.

The 4th galaxy candidate ($6^m.96$) is a more difficult case. The extinction-corrected colours are compatible with this being a real galaxy ($0^m.29, 0^m.91$) and it certainly has the appearance of a galaxy, looking like a spiral with a clear bulge and LSB disc – or a central bright star with some nebulosity around it. The optical does not provide clarification either. However, if it were a large spiral galaxy (which then should have $B^o \sim 9^m.0$) it should be visible on the blue (IIIaJ) and red sky survey plate at an extinction of "only" $A_B = 4^m.5$. There is no evidence for that at all on the respective optical sky survey plates. Hence we doubt it to be real.

The 5th object ($K_{20}^o = 6^m.99$) is clearly disqualified based on extinction-corrected colours alone ($0^m.23, -0^m.06$). It is also improbable given the thick dust layer ($A_B = 24^m.69$) through which it has been observed. However, it looks like a possible galaxy on the 2MASX image with a bright centre and LSB disc, despite its blue $(J - K)^o$ colour. Here, the optical image provides additional help. It shows the target to be a nebular object with a star at its centre. Interestingly this is also a strong radio continuum source.

The 6th galaxy in the list (with $7^m.05$) is a very obvious and bright galaxy at only intermediate extinction levels in the Puppis area. It is catalogued as ESO 430-G028 in the ESO Uppsala and ESO-LV catalogues (Lauberts 1982; Lauberts & Valentijn 1989). But being an S0 galaxy, it is clear why it was not detected with our H I observation. In fact, it does not even have a published redshift yet.

The colours ($-0^m.19$; $-0^m.49$)and high extinction level extinction ($A_B = 18^m.8$) of the 7th galaxy ($K_{20}^o = 7^m.18$) make it completely unrealistic for this to be a galaxy. Again visual inspection of both the NIR and optical image confirms this. The object looks like a star forming region with resolved individual stars and some reddish nebulosity around it in 2MASS whereas the optical shows none of these resolved stars, only a few stars (probably foreground) on a nebula (probably a reflection nebula). This also is a strong radio source.

The subsequent objects further down on this magnitude list ($K_{20}^o > 8^m.0$) are mostly definite galaxies, with only a minor fraction of uncertain or unlikely galaxies. The majority of these unlikely galaxies have extinction-corrected colours that are incompatible with these being galaxies obscured – and reddened – by the Milky Way, as they are quite blue.

So the relative lack of detections of intrinsically bright 2MASX objects in our sample can be understood.

5.2. Near-infrared colours of the galaxy sample

Figure 6 displays the observed and extinction-corrected $H - K$ vs. $J - K$ colour–colour diagram for the 2MASS galaxy sample. The cross gives an indication of the mean colours for unobscured galaxies as given in Jarrett et al. (2003), namely $H - K = 0^m.27$

and $J - K = 1^m.00$, which has a notoriously low dispersion about the mean. Only the late type Sd to Sm spirals have clearly lower colours (dipping to $0^m.7$ and $0^m.15$ for $J - K$ and $H - K$, respectively). Such bluish low surface brightness galaxies will, however, have entered our sample only in small numbers for the earlier mentioned reasons.

A comparison between the four panels allows some interesting observations. The colour plots uncorrected for extinction (top) are, as expected, quite similar as the extreme blueish objects were eliminated from the observing list, but no discrimination against reddened objects was made because of the foreground Galactic dust reddening. When correcting the colours for extinction, the detected galaxies (left bottom panel) fall quite nicely within the expected colour range for galaxies. The data points are, however, not distributed in a Gaussian cloud but rather in a more elongated linear distribution along the line of reddening. This can be explained by an over- or underestimate in the adopted extinction corrections. The likelihood for an overestimate is larger (independently confirmed in Sect. 5.5.) given that a larger fraction of the galaxies lie above the mean of unobscured galaxies as found in Jarrett et al. (2003) in the extinction-corrected colour–colour diagram.

This also holds for a large fraction of the non-detections. However, there are over a dozen extremely blue objects (three blue objects fall beyond the axes limits displayed in Fig. 6, with the most extreme having colours of $(H - K)^o = -0^m.64$ and $(J - K)^o = -1^m.68$, and one with extreme red $(H - K)^o$ colours). These objects clearly cannot be extragalactic.

The two most extreme sources (2MASX J07300453-1833166 and 2MASX J07300594-183254) lie at extinction levels of $A_B \sim 80$ mag (according to the Schlegel et al. 1998 maps), which even in the K_s band implies over 7 mag of extinction. Indeed, visual inspection of the NIR images as well as the optical images, find these two objects to be stars within H II regions, i.e. point-like objects with some fuzziness around them that emit strongly in the H-band. The same holds for most of the other objects. They are either stars that are located in or associated with an H II region, or some filamentary Galactic nebulosity (e.g. 2MASX J23352762+6452140) generally visible in both the optical and infrared, or the image is heavily contaminated by a very bright nearby star, and the resulting galaxy classification highly uncertain (e.g. 2MASX J20491597+5119089 with colours of $(H - K)^o = 4^m.34$ and $(J - K)^o = 0^m.27$).

Indeed, the galaxy with the bluest colours that was actually detected in H I (N17; with $0^m.07$ and $0^m.59$) is the first of the targeted objects in a list of increasing $(J - K)^0$ colour that actually has the appearance of a galaxy on NIR and optical images, and its properties. This observation is independently confirmed by Jarrett who visually examined all 2MASX sources within ±10° of the Galactic plane (priv. comm.) and classified most of these objects bluer than N17 as non-galaxies.

The lesson learned from these results indicate that the H I detection rate of 2MASS-selected ZoA galaxies can be significantly improved if, in addition to the exclusion of galaxy candidates with observed blue NIR colours $J - K$ and $H - K$, 2MASS objects are also excluded that have *extinction-corrected colours* $(J - K)^0 < 0^m.5$ and $(H - K)^0 < 0^m.0$.

The easiest way to apply such corrections is by systematically using the DIRBE extinction maps. Although we do find (see Sect. 5.5) – like many others (Schröder et al. 2007, and references therein; Cluver et al. 2008) – that when taking the DIRBE extinction measures at face value in southern ZOA studies, these seem overestimated by about 15% to 50% (Nagayama et al. 2004; Schröder et al. 2007; Tagg 2008; Cluver 2008).
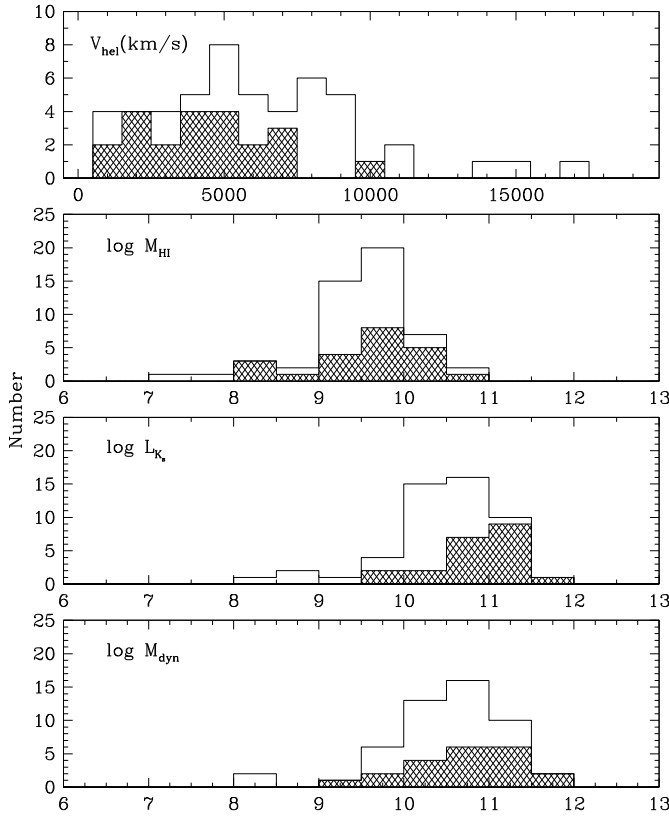
Fig. 7. Histograms of the distribution of the radial velocity, the total H I mass M_{HI} in $M_\odot$, Galactic extinction-corrected K_{20}^o band luminosity L_K, in $L_{\odot,K}$, and the dynamical mass M_{dyn}, also in solar units, of the galaxies detected at Nançay (shaded area) and Arecibo.

This overestimate will, however, have only a minimal effect on the extinction-corrected colours, as the selective reddening of $f_{J-K} = 0.12A_B$ for $J - K$ and $f_{H-K} = 0.05A_B$ for $H - K$ will reduce the colours by a relatively low amount. For instance, a reduction by an intermediate overestimate of 30% of the DIRBE extinction values and an intermediate to high ZoA dust column density of $A_B = 5^m.0$ results in a decrease of the extinction-corrected colour by the relative modest amount of $(J - K)^0 = 0^m.36$ and $(H - K)^0 = 0^m.07$.

If such an extinction-corrected colour limitation is then followed by visual examination of the individual and combined JHK_s images, partly in combination with optical images to help eliminate Galactic objects, cirrus, filaments and blended images, then a fairly high H I detection rate should be guaranteed given that spiral galaxies are generally more common than early type galaxies – even if we cannot discriminate against morphological type with NIR colours.

5.3. Global properties of the detected galaxies

In the following, we have a brief look at the distribution of the global properties of the detected galaxies such as radial velocity, K_s-band luminosity $L_{K_{20}}$, total H I mass M_{HI}, and dynamical mass M_{dyn} – see the resulting histograms in in Fig. 7. The hashed histograms denote the Nançay observations and the clear ones the Arecibo detections.

The velocity distribution of the Nançay detections shows galaxies out to about 7000 km s^{-1}, but beyond that its efficiency drops quite rapidly toward the velocity search limit of

V_{hel} = 11 825 km s^{-1}. This is very similar to the systematic southern Parkes HIPASS ZoA survey (Kraan-Korteweg et al. 2005, see their Fig. 2), which has similar instantaneous velocity coverage with a slightly lower sensitivity limit (rms = 6 mJy), except for the prominent peaks in their survey due to the crossing of the Hydra/Antlia filament and Great Attractor Wall (centred at about 3000 and 5000 km s^{-1} respectively). This suggests that a systematic H I follow-up of 2MASX ZoA objects – with the current setup of the Nançay pilot project observations – would be quite complementary to the southern ZoA efforts. Apart from the systematic ("blind") ZoA ALFA survey undertaken for the declination range visible with the Arecibo telescope (e.g. Henning et al. 2008; Springob 2008), no such efforts are currently being undertaken for the northern ZoA.

The present Arecibo detections have a higher mean velocity Peak – the majority lie between 5000 10 000 km s^{-1} with a handful of galaxies up to 18 000 km s^{-1}. The fact that very few galaxies have been detected at low velocities is – as mentioned in Sect. 5.1 – due to the work of Pantoja et al. (1997) who have already observed most of the (optically) larger galaxies at Arecibo in their efforts to map the southwestern spur of the Perseus-Pisces complex across the ZoA. Their sample peaked around the distance of this large-scale structure, namely 4250–8000 km s^{-1}. For comparison the detection rate of their nearer, optically visible, and partly classifiable into rough morphological type, is 53% for the 369 galaxy candidates targeted for observation, compared to our 35% of 2MASX selected Arecibo galaxies without previous redshift information. Their average noise was 1.3 ± 0.5 mJy, comparable to our observations.

Both (our work and Pantoja's) are considerably deeper than the ALFA precursor observations of 5–6 mJy rms sensitivity. Then again, the multibeam ALFA blind survey observations are powerful in that they do not require any previous identification of optical or NIR counterparts. They will therefore be much more efficient for nearby gas rich dwarfs at the highest extinction levels. In that sense, the Arecibo data presented here are complementary to the ALFA survey, at least for the Galactic anti-centre part of the ZoA visible from Arecibo (with relatively low extinction and star density).

The H I mass distribution is without further surprises. The Arecibo data find on average more H I-massive galaxies compared to Nançay, which is the effect of the galaxies being more distant on average. The overall H I-mass distribution is quite similar to the (as yet mostly unpublished) deep Parkes H I ZoA surveys (RCKK for the ZoA team; see also Donley et al. 2005, for the northern extension; Shafi 2008, for the Galactic Bulge extension) with the majority of galaxies lying in the range of 9–10.5 log M_{HI} ($M_\odot$) with a few outliers down to lower masses of a few times $10^7 M_\odot$, and two above that range ($>3 \times 10^{10} M_\odot$). Both the faintest and most massive galaxy are peculiar and discussed in further detail in Sect. 4.3.

The K_s-band luminosity distribution is not dissimilar to the H I-mass distribution except for an overall shift of one dex in the logarithmic solar units scale. This implies that the overall H I-mass to K_s-band light ratio has a mean of about 0.1, which corresponds closely to other surveys. The more nearby Nançay objects have a slightly lower M_{HI}/L_K compared to the Arecibo observations, due to the slightly different selection criteria, with the more distant, small and compact Arecibo galaxies more likely to be high surface brightness massive spirals.

The estimated dynamical masses are smaller than the combined stellar and gas masses for many of the galaxies. There are several biases contributing to this problem that stem from the location of these galaxies in the ZoA. Extinction effects are
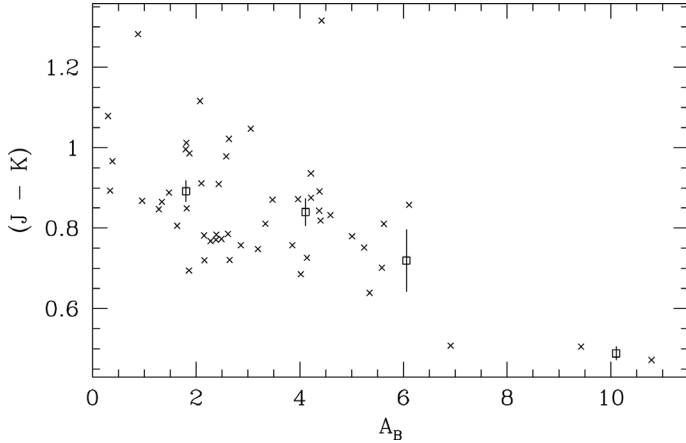
Fig. 8. Extinction-corrected $(J - K)^0$ colours of the H I detected galaxies as a function of the Galactic foreground B-band extinction correction factor in their direction, A_B, as estimated by Schlegel et al. (1998).
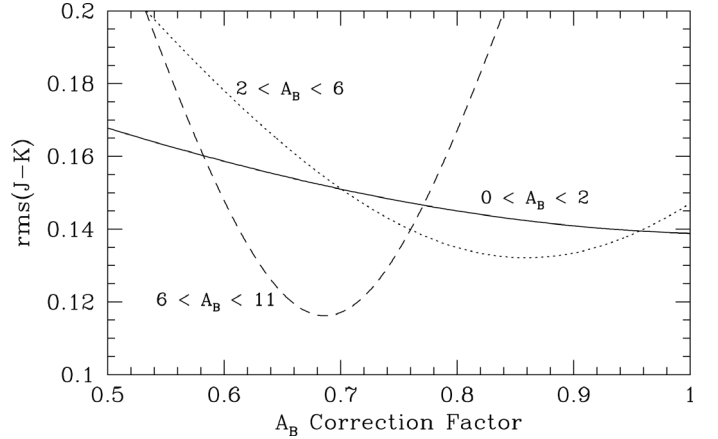

Fig. 9. Results of the search for the adjustments to the Galactic B-band extinction correction factor, A_B, as estimated by Schlegel et al. (1998), that would give the least scatter about the expected mean $J - K$ colour of the H I detected galaxies. The galaxies were divided into 3 bins, with A_B extinction correction factors between 0–2 mag, 2–6 mag, and 6–12 mag.

probably not the main cause of this problem: although the isophotal radii of the galaxies are underestimated, so too are the total K_s-band luminosities. In fact, by pushing the effective isophotal surface brightness fit to a higher level (like for a less obscured galaxy), the axis ratio would be measured closer to the bulge and likely to be rounder than if it were measured farther out in the disc (e.g. Cameron 1990). After correcting for inclination effects, this would generally lead to an overestimate of the dynamical mass.

The more likely explanation therefore is that the stellar confusion is the culprit. Unidentified faint stars, which are plentiful at these low latitudes, can add to the K_s-band light and distort the shape of the galaxy isophotes. The latter effect would diminish the inclination correction to the rotation velocities, which has a strong effect on our dynamical mass indicator.

5.4. Extinction model tests

The galaxies detected in this study mostly have H I masses in the range of 10^9 to 10^{10} $M_\odot$ (see Fig. 7), typical of other H I studies (e.g., Roberts & Haynes 1994), and the galaxies generally show no obvious trends as a function of redshift or local extinction. However, after applying extinction corrections at J and K_s, and the minor corrections to the $J - K$ colours for redshift (Table 2 and 5, Col. 5), we still find that the galaxies grow successively redder in regions of higher estimated extinction – as suggested already in Sect. 5.2 (Fig. 6). Figure 8 shows a plot of corrected $(J - K)^o$ colour as a function of the value of A_B estimated by Schlegel et al. (1998). This effect has been noted for other ZoA galaxies (Nagayama et al. 2004; Schröder et al. 2007; Tagg 2008; Cluver 2009), who find overestimates of $f(A_\lambda^{real}/A_\lambda^{obs}) = 0.67, 0.87, 0.75$, and 0.84, respectively, of the values implied by Schlegel et al. (1998). The thorough analysis by Schröder et al. (2007) derived by optimising this factor in fitting all three DENIS NIR colours IJK simultaneously to medium to highly obscured ZoA galaxies finds that reducing the extinction corrections by about 15% introduces less bias as a function of A_B.

Since our galaxies should intrinsically have typical $J - K$ colours of about $0.^m9$, we performed the following test. We selected the galaxies with A_B extinctions in the ranges of 0–2, 2–6, and 6–12 mag, respectively, and searched for the value of the adjustment to the Schlegel et al. values that would give the least scatter about the expected mean colour. The results of this test

are shown in Fig. 9 where the curves show that the scatter of the colour is minimized at approximately the Schlegel et al. (1998) extinction values for moderate extinction – which generally are at $|b| \gtrsim 5°$, where the Schlegel et al. values are indeed said to still be valid, whereas in regions of moderate extinction this reduces to 86% of the Schlegel et al. values, and to about 69% for our most heavily-extincted galaxies. This falls well within the range of other ZoA studies. As previous studies were mostly restricted to the southern sky, it is reassuring to notice that this effect for our mostly northern sample seems to be of the same order in the southern sky.

This trend suggests that either the Schlegel et al. (1998) extinctions are overestimated in the most-highly extincted regions or that the relative infrared extinction is less in these regions.

5.5. Indications of large-scale structures connections

Although this is a pilot project, and the number of newly measured redshifts of obscured galaxies is relatively small ($N = 51$), we nevertheless had a look at their distribution in redshift space to see what kind of structures they trace across the ZoA or what new large-scale features they might hint at. The locations of these new H I detections are shown in Fig. 10. Their positions on the sky are plotted as square symbols in four radial velocity slices (or shells) of 3000 km s^{-1} width for the velocity range 0–12 000 km s^{-1} (the 3 even higher velocity detections are not displayed). They are superimposed on the distribution of galaxies with previously measured redshifts, as obtained from HyperLeda. The colour coding refers to the different redshift ranges within a slice, with red marking the nearest, dark blue the middle and the fainter cyan the most distant $\Delta V = 1000$ km s^{-1} interval per slice. The black lines demarcate the southern Nançay ($-40°$) and Arecibo ($0°$) observable declination limits.

The magenta boxes outline the survey coverage of the various deep ZoA H I-surveys (rms = 6 mJy) centred on the southern Galactic plane undertaken with the multi-beam receiver of the Parkes 64m radio telescope (see Kraan-Korteweg et al. 2008, for survey details). The displayed data points also include the more shallow HIPASS survey results (Meyer et al. 2004; Wong et al. 2006). Note again that there is little overlap between our survey and this southern one, partly because of our selection of northern
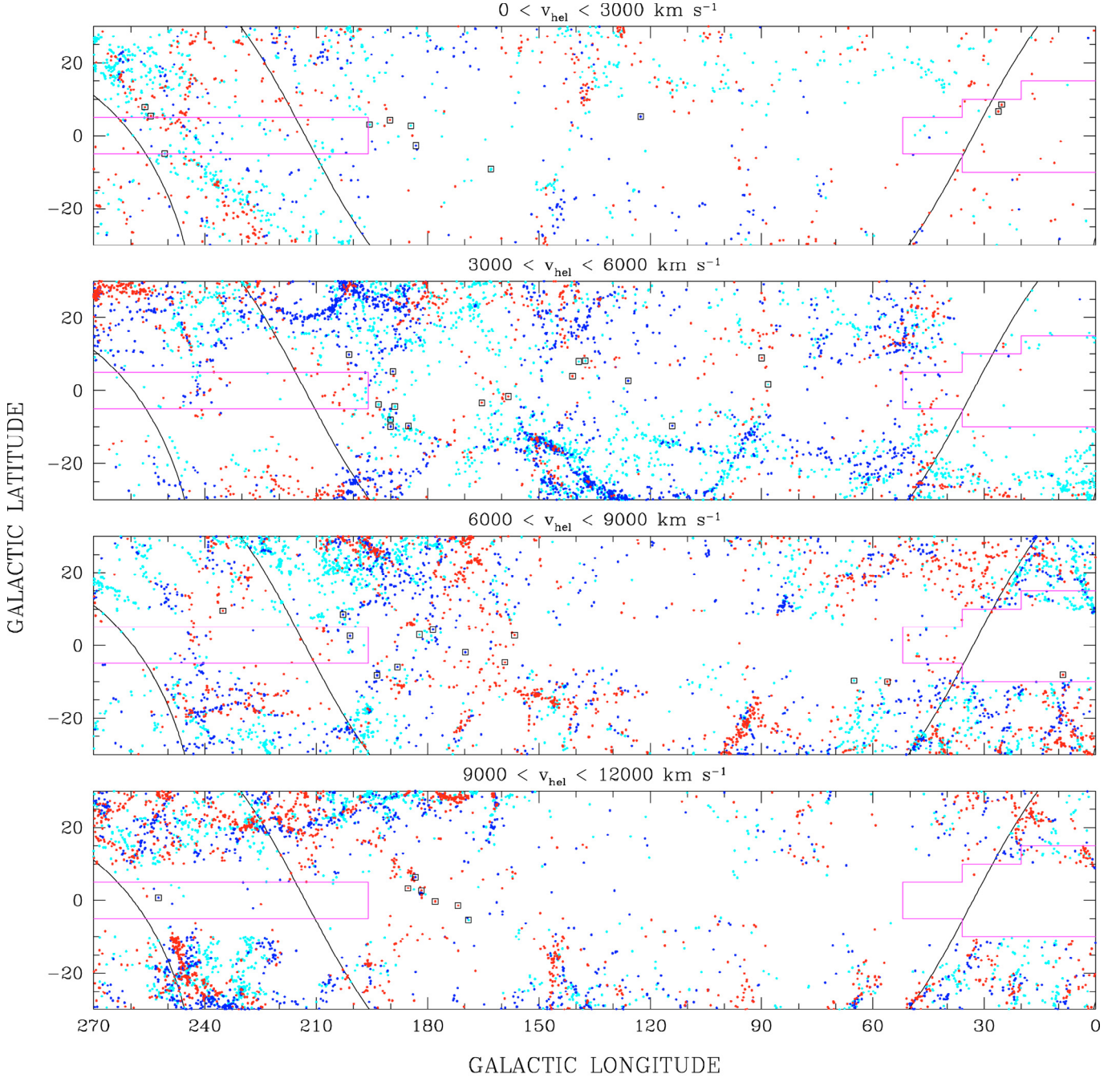
Fig. 10. Plots showing our H I detections (black squares) superimposed on known large-scale structures (as available in HyperLeda) in four radial velocity intervals (0–3000, 3000–6000, 6000–9000 and 9000–12 000 km s^{-1}) in Galactic coordinates. Within each 3000 km s^{-1} slice in radial velocity, the galaxies in the nearest 1000 km s^{-1} wide bin are shown in red, the middle 1000 km s^{-1} in dark blue, and the furthest 1000 km s^{-1} in light blue. The dark lines indicate declinations of $\delta = 12°$ as well as $\delta = -40°$ the southern declination limits of, respectively, our Arecibo and Nançay samples. The outlined boxes denote the deep H I surveys undertaken with the Parkes MultiBeam Receiver. Note that overlap with these surveys was minimal.

telescopes, and partly because 2MASS does not uncover galaxies in the high star-density around the wider Galactic bulge area (Fig. 9 in Kraan-Korteweg 2005).

Overall, the new detections are mostly seen to follow the filamentary structures. We will comment on the detection slice by slice by comparing them to known structures, the northern, very shallow (40 mJy, $V < 4000$ km s^{-1}) H I Dwingeloo obscured galaxy survey (DOGS; e.g. Henning et al. 2000a), the 2MASX redshift survey (2MRS) Wiener filter density field

reconstructions (2M-WF, Erdogdu et al. 2006b), as well as the most recent 2MASX photometric redshift slices (2MX-LSS; Jarrett 2008 – see http://web.ipac.caltech.edu/staff/jarrett/lss/index.html).

Top panel (0 km s^{-1} < V$_{hel}$ < 3000 km s^{-1}): the galaxies around $\ell \sim 240°$ clearly form part of the well-established nearby Puppis filament, whereas the detections clumped around 180°–200° are more of a mystery. They seem to lie in a fairly underdense region. Interestingly enough, the 2M-WF

reconstruction finds a clear unknown overdensity (called C5) in this region which is also notable in the respective 2M-LSS slice. This region and overdensity might be worthwhile pursuing further. No new galaxies were detected at the super-Galactic plane (SGP) crossing (at ~140°) though some are visible in the next panel. The two galaxies at about 30° must form part of a nearby filamentary structure identified for the first time in the Parkes multibeam Galactic bulge extension survey (Kraan-Korteweg et al. 2008; Shafi 2008) that protrudes into the local void.

Second panel (3000 km s⁻¹ < V_{hel} < 6000 km s⁻¹): the two detections at both ~160° and ~90° are clearly connected with the Perseus-Pisces (PP) complex. The connection across the ZoA leading from Perseus to A569 is very strong in the 2M-WF reconstructions as well as evident in the 2M-SS slice, more clearly so in the heavily smoothed display. The two other galaxies belong to the south-western spur of the PP complex, which was also found by 2M-WF and 2M-LSS. Both the detections at ~190° slightly below the plane) and ~140° (above the plane) show a prominent signal in 2M-WF (marked as OR for Orion and CAM for Cameleopardis there). While visible in 2M-LSS it is less obvious there, though more so in the smoothed version.

Third panel (6000 km s⁻¹ < V_{hel} < 9000 km s⁻¹): two clouds of detections can be attributed to known, or rather suspected, structures. The two galaxies at ~190° (below the plane) also seem part of Orion (OR), as this has an even stronger signal in the reconstructed density field in 2M-WF for this redshift range. The other galaxies seem to follow the main PP-chain.

Bottom panel (9000 km s⁻¹ < V_{hel} < 12 000 km s⁻¹): six of the 7 detections are remarkably aligned and seem to suggest some kind of filament – or the far end of the sheet-like PP-chain? Such a feature is not recovered in the 2M-WF, however, though it is evident in the 2M-LSS slices. It might be worthwhile to observe more galaxies in this velocity range to verify whether this truly is a previously unknown filament.

6. Conclusions

To complement ongoing "all-sky" redshift surveys to map extragalactic large-scale structures in the nearby Universe and improve our understanding of its dynamics and observed flow fields, we undertook a pilot project to obtain H I observations of about 200 optically obscured or invisible galaxy candidates behind the Milky Way ($|b| < 10°$), the zone of avoidance strip generally avoided in such surveys. Likely galaxy sources were extracted in 2000–2002 from the 2MASS extended source catalog (2MASX), then a database under construction. This near-infrared (NIR) catalogue penetrates the ZoA to considerably lower extinction levels than optical ones. For this we used both the Nançay and Arecibo radio telescopes.

Apart from excluding extremely blue objects, no further selection criteria were applied, as near-infrared galaxy colours show hardly any dependence on morphology. Furthermore, the NIR galaxy colours are affected quite strongly by the varying Galactic dust column density through which the galaxies are viewed.

The overall detection rate of the 185 observed 2MASX galaxies whose spectra were not affected by nearby continuum sources is quite low: 24% and 35% for the Nançay and Arecibo samples respectively This detection rate is lower than for H I-follow-ups of optically selected galaxies, even in the ZoA. For instance, a similar H I survey of optically selected ZoA galaxies (Kraan-Korteweg et al. 2002) reached a 44% detection rate (though a pre-selection on morphological type favouring spiral galaxies was made).

Despite this relatively low detection rate, it should be noted that other means of obtaining redshifts (optical spectroscopy) for galaxies hidden by the Milky Way remain extremely difficult due to their reduced surface brightness. H I observations of galaxy candidates still remain the most efficient tool in mapping large-scale structures across the ZoA.

In addition, this pilot survey taught us that a significant number of the non-detections could have easily been excluded from the observing list by:

(a) examination of the composite *JHK* images of the *extinction-corrected* brightest sources (now easily available), in combination with the higher-resolution optical SDSS images (when available – which is rarely the case for the present sample). Most of the extended objects with $K^o \gtrsim 7.^m0$ or $7.^m5$ could readily be dismissed as galaxy candidates in that way (see Fig. 5 and Sect. 5.1);

(b) considering *extinction-corrected* colour limits. All objects that were bluer than $(J - K)^0 < 0.^m5$ and $(H - K)^0 < 0.^m0$ (Fig. 6) were found to be Galactic objects, mostly H II regions or filamentary structures associated with Galactic objects (Sect. 5.5).

Based on these two criteria the total number of Nançay sources observed would have been reduced by 15%, to 99 instead of 116: 11 on their images alone, 6 just on their colour, and 7 on both. None of these 17 objects were detected in H I. The smaller and fainter Arecibo sources are not really adequate for rejection through NIR image examination, as the largest and brightest ones in the area had already been observed in H I by Pantoja et al. (1994, 1997). Only two of them would have been rejected based on their colours.

The Schlegel et al. (1998) Galactic extinction values serve as a good first proxy for these tests, even though they are not calibrated at the lowest Galactic latitudes ($|b| \leq 5°$). An extinction overestimate will have a minimal effect on the verification procedures, or even on the extinction-corrected colours delimitations as the selective reddening will reduce the colours by only a relatively low amount of $0.12A_B$ and $0.05A_B$ for $J - K$ and $H - K$ respectively.

The NIR colours of the detected galaxies were actually used to assess the accuracy of the DIRBE extinction values at low latitudes if taken at face value. The results confirm that the values from Schlegel et al. (1998) are valid for latitudes above $|b| \gtrsim 5°$, whereas in regions of moderate extinction this reduces to 86%, and to 69% for our most heavily-extincted galaxies. It is reassuring that these values (from our mostly northern sky sample) seems in good agreement with the previous mostly southern sky derivations (e.g., Schroeder et al. 2007, and references therein).

Overall, the properties of the detected galaxies match those of other surveys. The sample is too sparse yet to give an improved insight into suspected or unknown large-scale structures behind the Milky Way. However, the detections already indicate (see Fig. 10) that a further probing of the galaxy distribution will quantify filaments, clusters and also voids in this part of the ZoA.

Hence our H I detection rate of 2MASS-selected ZoA galaxies can be significantly improved, if the above mentioned image examinations and extinction-corrected limits are employed. Such a systematic survey would actually be a worthy pursuit, as it would be complementary to the ongoing "blind" deep ZoA H I Parkes multi-beam survey (at $|b| \leq 5°$; of similar velocity coverage though slightly lower sensitivity than the Nançay pilot project), if done for the ZoA in the latitude range of $5° \leq |b| \leq 10°$ accessible to Nançay, and for the northern ZoA at $|b| \leq 10°$

in the areas not covered by the Arecibo ALFA surveys ($\delta > 35°$). We intend to pursue such a survey at Nançay.

References

Allen, C. W. 1973, Astrophysical Quantities (London: Athlone Press)

Andreon, S. 2002, A&A, 382, 495

Cameron, L. M. 1990, A&A, 233, 16

Cardelli, J. A., Clayton, G. C., & Mathis, J. S. 1989, ApJ, 345, 245

Cluver, M. E. 2009, Ph.D. Thesis, University of Cape Town

Cluver, M. E., Jarrett., T. H. Appleton, P. N., et al. 2008, ApJ, 686, 17L

Chamaraux, P., Masnoux, J. L., Kazès, I., et al. 1999, MNRAS, 307, 236

Colina, L., & Bohlin, R. 1997, AJ, 113, 1138

de Vaucouleurs, G., de Vaucouleurs, A., Corwin, H. G., et al. 1991, The Third Reference Catalogue of Bright Galaxies (New York: Springer-Verlag) (RC3)

Donley, J. L., Staveley-Smith, J. L., Kraan-Korteweg, R. C., et al. 2005, AJ, 129, 220

Donley, J. L., Koribalski, B. S., Staveley-Smith, J. L., et al. 2006, MNRAS, 369, 1741

Erdogdu, P., Huchra, J. P., Lahav, O., et al. 2006a, MNRAS, 368, 1515

Erdogdu, P., Lahav, O., Huchra, J. P., et al. 2006b, MNRAS, 373, 45

Fisher, J. R., Huchra, J. P., Strauss, M. A., et al. 1995, ApJS, 100, 69

Fouqué, P., Bottinelli, L., Durand, N., Gouguenheim, L., & Paturel, G. 1990, A&AS, 86, 473

Henning, P. A., Rivers, A. J., & Staveley-Smith, L. 2000a, in Mapping the Hidden Universe, ed. R. C. Kraan-Korteweg, P. A. Henning, & H. Andernach, ASP Conf. Ser., 218, 61

Henning, P. A., Staveley-Smith, L., Ekers, R. D., et al. 2000b, AJ, 119, 2686

Henning, P. A., Springob, C. M., Day, F., et al. 2008, in The Evolution of Galaxies through the H I window, ed. R. Minchin, AIP Conf. Proc., 1035, 246

Roberts, M. S., & Haynes, M. P. 1994, ARA&A, 32, 115

Huchra, J., Davis, M., Tonry, J., & Latham, D. 1983, ApJS, 52, 89

Huchra, J., Jarrett, T., Skrutskie, M., et al. 2005, in Nearby Large-Scale Structures and the zone of avoidance, ed. A. P. Fairall, & P. A. Woudt, ASP Conf. Ser., 329, 135

Huchtmeier, W. K., Karachentsev, I. D., Karachentseva, V. E., et al. 2005, A&A, 435, 459

Jarrett, T. H., Chester, T., Cutri, R., et al. 2000, AJ, 120, 298

Jarrett, T. H., Chester, T., Cutri, R., et al. 2003, AJ, 125, 525

Karachentseva, V. E., & Karachentsev, I. D. 2000, A&AS, 146, 359

Kirby, E. M., Jerjen, H., Ryder, S. D., & Driver, S. 2008, AJ, 136, 1866

Kraan-Korteweg, R. C. 2005, RvMA, 18, 48

Kraan-Korteweg, R. C., & Lahev, O. 2000, ARA&A, 10, 211

Kraan-Korteweg, R. C., Henning, P. A., & Schröder, A. C. 2002, A&A, 391, 887

Kraan-Korteweg, R. C., Staveley-Smith, L., Donley, J., Koribalski, B., & Henning, P. A. 2005, in Maps of the Cosmos, ed. M. Colless, L. Staveley-Smith, & R. Stathakis, ASP Conf. Ser., 216, 203

Kraan-Korteweg, R. C., Shafi, N., Koribalski, B., et al. 2008, in Galaxies in the Local Volume, ed. B. Koribalski, & H. Jerjen, ApSS, 13

Lauberts, A. 1982, The ESO/Uppsala Survey of the ESO (B) (ESO, Garching)

Lauberts, A., & Valentijn, E. A. 1989, The surface photometry catalogue of the ESO-Uppsala galaxies (ESO, Garching)

Lewis, B. M. 1983, AJ, 88, 962

Loeb, A., & Narayan, R. 2008, MNRAS 386, 2221L

Masters, K. L., Springob, C. M., & Huchra, J. P. 2008, AJ, 135, 1738

McGaugh, S. S., Schombert, J. M., Bothun, G. D., & de Blok, W. J. G. 2000, ApJ, 533, L99

Matthews, L. D., & van Driel, W. 2000, A&A, 143, 421

Meyer, M. J., Zwaan, M. A., Webster, R. L., et al. 2004, MNRAS, 350, 1195

Monnier Ragaigne, D., van Driel, W., Schneider, S. E., Jarrett, T. H., & Balkowski, C. 2003a, A&A, 405, 99

Monnier Ragaigne, D., van Driel, W., Schneider, S. E., Balkowski, C., & Jarrett, T. H. 2003b, A&A, 408, 465

Nagayama, T., Woudt, P. A., Nagashima, C., et al. 2004, MNRAS, 354, 980

Pantoja, C. A., Altschuler, D. R., Giovanardi, C., & Giovanelli, R. 1994, in Unveiling Large-Scale Structures Behind the Milky Way, ed. C. Balkowski, & R. C. Kraan-Korteweg, ASP Conf. Ser., 67, 143

Pantoja, C. A., Altschuler, D. R., Giovanardi, C., & Giovanelli, R. 1997, AJ, 113, 905

Paturel, G., Fouqué, P., Bottinelli, L., & Gouguenheim, L. 1989, A&AS, 80, 299 (PGC)

Paturel, G., Bottinelli, L., Di Nella, H., et al. 1997, A&AS, 124, 109

Paturel, G., Petit, C., Prugniel, P., et al. 2003a, A&A, 412, 45

Paturel, G., Theureau, G., Bottinelli, L., et al. 2003b, A&A, 412, 57

Saunders, W., Sutherland, W. J., & Maddox, S. J. 2000, MNRAS, 317, 55

Schlegel, D. J., Finkbeiner, D. P., & Davis, M. 1998, ApJ, 500, 525

Schneider, S. E., Helou, G., Salpeter, E. E., & Terzian, Y. 1986, AJ, 92, 742

Schneider, S. E., Thuan T. X., Magri, C., & Wadiak, J. E. 1990, ApJS, 72, 245

Schröder, A. C., Mamon, G. A., Kraan-Korteweg, R. C., & Woudt, P. A. 2007, A&A, 466,481

Shafi, N. B. 2008, MSc Thesis, University of Cape Town

Skrutskie, M. F., Cutri, R. M., Stiening, R., et al. 2006, AJ, 131, 1163

Springob, C. M., Henning, P. A., Catinella, B., et al. 2008, in Dark Galaxies and Lost Baryons, ed. J. I. Davies, & M. J. Disney, IAU Symp., 244, 383

Tagg, J. 2008, MSc Thesis, University of Cape Town

Takata, T., Yamada, T., Saito, M., Chamaraux, P., & Kazès, I. 1994, A&AS, 104, 529

Theureau, G., Bottinelli, L., Coudreau-Durand, N., et al. 1998, A&AS, 130,333

Tonry, J. L., Blakeslee, J. P., Ajhar, E. A., & Dressler, A. 2000, ApJ, 530, 625

van Driel, W., Pezzani, J., & Gérard, E. 1997, in High-sensitivity Radio Astronomy, ed. N. Jackson, & R. J. Davies (Cambridge: Cambridge Univ. Press) 229

Wegner, G., Bernardi, M., Willmer, C. N. A., et al. 2003, AJ, 126, 2268

West, R. M., Surdej, J., Schuster, H.-E., et al. 1981, A&AS, 46, 57

Wong, O. I., Ryan-Weber, E. V., Garcia-Appado, D. A., et al. 2006, MNRAS, 371, 1855